Chapter 2

Silicon Nanowires for Real-Time, Label-Free Biological Sensing

2.1 Introduction

Over the past few years a number of new biomolecular sensors have been reported.[1–5] The development of these devices is in part driven by the emerging needs of both systems biology[6, 7] and personalized and predictive medicine[8]—both of which are increasingly requiring quantitative, rapid, and multiparameter measurement capabilities on ever smaller amounts of tissues, cells, serum, etc. To meet these needs, many groups have focused their attention on developing real-time, highly sensitive, and potentially scalable tools for detecting nucleic acids and proteins. One-dimensional nanostructures such as nanotubes,[9–12] semiconductors,[13–15] metal oxide nanowires (NWs),[16] and conducting polymer nanofilaments[17] have all been demonstrated as capable of the label-free detection of small molecules, nucleic acids, and proteins.

Silicon nanowire (SiNW) biosensors are promising label-free, electronic-based detectors of biomolecules.[2] However, significant scientific challenges remain before SiNW sensors can be viewed as a realistic technology. One challenge relates to the use of these devices in biologically relevant media, which is typically a 0.14 M electrolyte. NW sensors detect the local change in charge density (and the accompanying change in local chemical potential) that characterizes a target/capture agent binding event. That changing chemical

potential is detected as a 'gating' voltage by the NW, and so, at a given voltage, affects the source (S) → drain (D) current value, or I_{SD}. However, that change is screened (via Debye screening) from the NW by the solution in which the sensing takes place.[18, 19] Debye screening is a function of electrolyte concentration, and in a 0.14 M electrolyte (which represents physiological environments such as serum) the screening length is about 1 nm.[20] Because of this, all reports on SiNW sensors for proteins or DNA have been carried out in low-ionic-strength solutions.[14, 15, 21] In this chapter, we demonstrate that a single-stranded complementary oligonucleotide is able to significantly change the conductance of a group of 20-nm-diameter SiNWs (p-doped at ~ 10^{19} cm^{-3}) in 0.165 M solution by hybridizing to a primary DNA strand that has been electrostatically adsorbed onto an amine-terminated organic monolayer atop the NWs. This intimate contact of the primary strand with the amine groups of the NW surface brings the binding event close enough to the NW to be electronically detected. In addition, within a 0.165 M ionic-strength solution the DNA hybridization is more efficient.[10, 22] However, we further demonstrate that the sensing of proteins in physiological conditions is fundamentally limited by the size of the antibodies, which, at the moment, remain the most widely used high-affinity probes for most proteins. This problem may be circumvented by utilizing alternative probes, which have smaller physical size, to circumvent the Debye screening issue. In this chapter, we also propose to use small peptides as a capture agent for protein sensing with NWs.

Synthetic capture agents such as peptides have advantages over macrobiomolecules including antibodies, nucleic acid aptamers, and protein aptamers.[23, 24] They are robust in terms of maintaining their structure and can be easier to produce and purify in bulk than antibodies or aptamers. Especially for NW-FETs, their small size enables detection of the

presence of target molecules in high-ionic-strength solution which has a short Debye screening length. Synthetic capture agents can also be immobilized on the surface in a defined manner, which means we can control the orientation of the capture agents in solution based on the reaction chemistries implemented. Recently, Heather et al. reported a methodology to find peptide-based protein-capture agents through iterative *in situ* click chemistry and one-bead-one-compound method.[25] Their approach has a high impact since it can be expected to create cheap but highly stable synthetic capture agents that have the potential to take the place of the antibodies.

To immobilize the peptide, we utilized the Cu^{I}-catalyzed alkyne-azide 'click' cycloaddition. Thus, we can expect all the peptides to be fully exposed to the solution in the same manner. Since the click reaction is defined by a set of stringent criteria such as selectivity, wide scope, high yields, and inoffensive by-products, it can easily serve as a general chemical method for biological applications.[26] As a demonstration of this approach, we used the FLAG system: FLAG peptides and monoclonal anti-FLAG M2 antibodies. The FLAG peptides are modified at the N-terminus with the alkyne and two spacer amino acids, SG, to increase accessibility of the target molecules.[24]

A second challenge involves demonstrating reproducible and high-throughput nanofabrication methods that can produce nearly identical NW sensors time and time again, and that allow for multiple measurements to be executed in parallel. Based on electrostatic considerations, it is well known that nanowires are more sensitive to surface charges than planar ion-sensitive field-effect transistors (ISFET) or chemical field-effect transistors (CHEMFET). Such dimensional arguments[27] imply that nontraditional methods must be utilized to fabricate the NWs.[28, 29] While biological sensing with silicon produced by wet

etch[30] or dry oxidation[31] was reported, to date, most reports of NW sensors have utilized semiconductor NWs grown as bulk materials[32] using the vapor-liquid-solid (VLS) technique.[33] This method produces high quality NWs, but they are characterized by a distribution of lengths and diameters, and they also must be assembled into the appropriate device structure (or the device structure must be constructed around the nanowire[34]). In this study we utilize the Superlattice Nanowire Pattern Transfer (SNAP) method[35] to produce highly aligned array of 400 SiNWs, each 20 nm wide and ~ 2 millimeters long. Standard semiconductor processing techniques are utilized to control the NW doping level,[36] to section the NWs into several individual sensor arrays, to establish electrical contacts to the NW sensors, and to integrate each array into a microfluidic channel. Such integration is rather challenging in itself;[37] however, it is extremely important for obtaining low-noise, reproducible measurements. The resulting NWs exhibit excellent, controllable, and reproducible electrical characteristics from device to device and across fabrication runs. The sensor platforms may also be fabricated in reasonably high throughput. A key advantage, which is provided by the top-down approach of SNAP vs. the bottom-up VLS technique, is the precise control of doping level of the nanowires. We utilize diffusion doping technique to create nanowires with well-characterized doping levels ranging from 10^{17} to 10^{20} cm^{-3}. We demonstrate that the doping level profoundly affects the limit of detection of both DNA and protein; therefore, nanowires can be tuned to a specific dynamic range window with an appropriate concentration of impurities.

A third challenge involves the SiNW surface. The effectiveness of SiNWs for biomolecular sensing arises in part because of their high surface-to-volume ratio. The native (1–2 nm thick) surface oxide on a SiNW may limit sensor performance due to the

presence of interfacial electronic states.[38, 39] In addition, the oxide surface of SiNWs acts as a dielectric which can screen the NW from the chemical event to be sensed. Covalent alkyl passivation of Si(111) surfaces can render those surfaces resistant to oxidation in air[40] and under oxidative potentials.[41, 42] Recently, methyl-passivated SiNWs were shown to exhibit improved field-effect transistor characteristics.[43] More complex molecules, such as amine-terminated alkyl groups, can be covalently attached to H-terminated Si surfaces (including SiNWs) via UV-initiated radical chemistry.[44–47] Such chemistry has been used for a covalent attachment of DNA to VLS-grown SiNWs.[48] DNA may also be immobilized on amine-terminated surfaces via electrostatic interactions. In this work, we explore how the characteristics of SiNW sensors vary as the nature of the inorganic/organic interface is varied. We find that SiNW sensors in which the native oxide provides the interface for organic functionalization are significantly inferior in terms of both sensitivity and dynamic range when compared with SiNW sensors that are directly passivated with an alkyl monolayer.

A final challenge is actually an opportunity that is provided by the intrinsic nature of a label-free, real-time sensor. The standard such sensing technique is surface plasmon resonance (SPR).[49] SPR is utilized to determine the κ_{on} and κ_{off} rates, and hence the equilibrium binding affinities, of complementary DNA strands or antibody–protein pairs. The capture agent (single stranded DNA or an antibody) is typically surface-bound, and so the key experimental variables are the analyte (complementary DNA strand or a protein), concentration, and time. If k_{on} and k_{off} are both known, then SPR can be utilized to quantitate the analyte concentration. Very few biomolecular sensing techniques are quantitative. In this work, we dope the NW sensors so that their sensing dynamic range is

optimized to match that of SPR for the detection of DNA hybridization or protein binding to an antibody. We demonstrate the equivalence of these two methods, and thus demonstrate the potential use of SiNW sensors for quantitating analyte concentrations. SiNW sensors can be optimized for significantly higher sensitivity than SPR by an appropriate surface modification and doping, and thus can potentially be utilized to quantitate the concentrations of specific biomolecules at very low concentrations. That would constitute a unique application of these devices.

2.2 Experimental Methods

2.2.1 Nanowire sensor fabrication

The SiNW arrays were fabricated as previously described,[50] and all fabrication was done within a class 1000 or class 100 clean room environment. A typical NW sensor device employed in this work for DNA sensing is shown in Fig. 2.1. The starting material for the SNAP process was an intrinsic, 320 Å thick silicon-on-insulator (SOI) substrate with (100) orientation (Ibis Technology Inc., Danvers, MA) and a 1500 Å buried oxide. Cleaned substrates were coated with either p-type (Boron A, Filmtronics, Inc. Bulter, PA) or n-type (Phosphorosilica, Emulsitone, Inc., Whippany, NJ) spin-on-dopants (SODs). SODs were thermally diffused into the SOI film. We reproducibly controlled the resulting substrate doping concentration, as quantified by 4-point resistivity measurements on the SOI film, by varying the diffusion temperature. For this study, a 3 min, 850°C (875^{o}C) rapid thermal anneal was used to generate p (n) dopant levels of ~ $8\times10^{18}/cm^{3}$. The p-type substrates

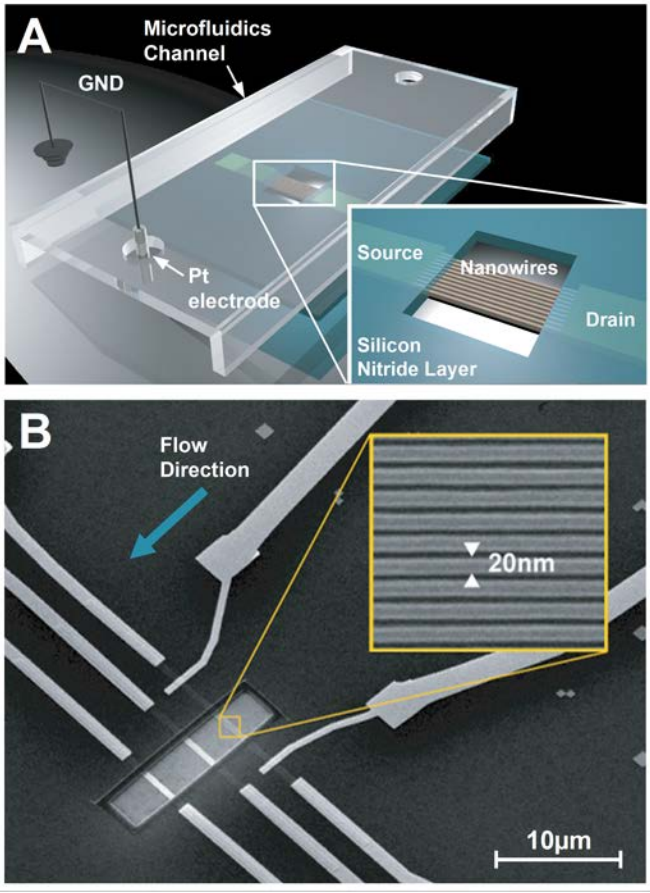

Figure 2.1 A diagram (A) and an SEM image (B) of a single device section containing three groups of ~ 10 SiNWs in a microfluidics channel. The wafer is covered with Si_3N_4 except for an exposed active region with SiNWs (A, inset; B). B, inset: High-resolution SEM image of 20 nm SiNWs

were thermally oxidized in O_2 for 1 min at 850°C, which was necessary to remove the organic SOD residue. The SOD films were removed by brief immersion in piranha (70% H_2SO_4, 30% H_2O_2), followed by a water rinse, and immersion in buffered oxide etchant (BOE; General Chemical, Parcippany, NJ).

The SNAP method for NW array fabrication translates the atomic control achievable over the individual layer thicknesses within an MBE-grown GaAs/$Al_xGa_{(1-x)}As$ superlattice into an identical level of control over NW width, length, and spacing. This method has been described in some detail elsewhere,[35, 50] and will not be described here. We utilized

the SNAP process to produce a 2-mm-long array of 400 SiNWs, each of 20 nm width and patterned at 35 nm pitch (Fig. 2.1B, inset).

The SiNWs were sectioned into ~ 30-μm-long segments using e-beam lithography (EBL) and SF_6 RIE etching, producing groups of ~ 10 SiNWs with a diameter of 20 nm. Six identical sections from a single imprint, each containing 3 NW segments, were produced. One such section is shown in Fig. 2.1. When fully integrated with the microfluidics channels, this allowed for six separate measurements, with three independent NW segments per measurement. Source (S) and drain (D) electrical contacts, ~ 500 nm wide and separated by 10–15 μm, were patterned using electron beam lithography (EBL) on each section of SiNWs. Prior to metallization, the native oxide of the SiNWs over the contacts was removed with BOE to promote the formation of ohmic contacts. Finally, 400 Å Ti and 500 Å Pt were evaporated to form S/D contacts. Immediately after the lift-off, the devices were annealed in 95% N_2, 5% H_2 at 475^{o}C for 5 min. This step greatly improves the characteristics of SNAP SiNW FETs. To provide room for a 1 cm by 1.5 cm PDMS chip with microchannels for analyte delivery to each section of the SiNWs (Fig. 2.1A and 2.2), the electrical contacts were extended to the edges of the substrate using standard photolithography techniques followed by evaporation of 200 Å Ti and 1500 Å Au. To eliminate parasitic current between metal contacts in solution, approximately 70 nm of Si_3N_4 was deposited using plasma-enhanced chemical vapor deposition (PECVD) everywhere on the chip except in 5 μm by 20 μm regions over the NWs and the outer tips of the Au contacts. Briefly, 100 nm of chromium was deposited over an active region of the NWs. PECVD was used to deposit Si_3N_4 film at 300°C (900 mT, 20 W, 13.5 MHz) from N_2 (1960 sccm), NH_3 (55 sccm), and SiH_4 (40 sccm) gases. The nitride film was selectively

etched with CHF_3/O_2 plasma over the protected NW region using PMMA as a mask, followed by the removal of chromium with CR-7C (Cyantek Corp., Fremont, CA).

Microfluidics Fabrication. The soft lithography microfluidics chips were fabricated as described by others.[51] We observed that manual introduction/changing of solutions caused serious noise, capacitive currents, and baseline shifts in real-time recordings. Thus, for low noise, stable, real-time electronic measurements, we found it necessary to automate fluid injection and solution switching by using PDMS multilayer, integrated elastomeric microfluidics chips of the type developed by the Quake and Scherer groups.[52] The size of the wafer containing SiNWs did not permit the inclusion of all necessary flow and control lines necessary for the fluidic handling chip, and so that was fabricated as a separate chip. Such PDMS chip was fabricated using a standard photolithography: mixed PDMS (Dow Corning, Inc., Midland, MI) was applied over a pre-made photoresist (Shipley SPR 220-7) molding on silicon wafer and incompletely cured at 80°C for 30 min. The chip containing microchannels was cut out of the PDMS layer and 0.5-mm-diameter holes were punctured to serve as microchannel inlets and outlets. The fluidic chip and the device containing SiNWs were then brought into contact, with the 100-μm-wide microchannels aligned over the individual nanowire sections. The assembled device was cured to completion overnight at 80°C.

To automate an injection/changing of analyte solutions, we also introduced a second PDMS chip which can sequentially inject four different solutions into one of six microchannels on the silicon wafer. Such sample injection chip is composed of two layers,

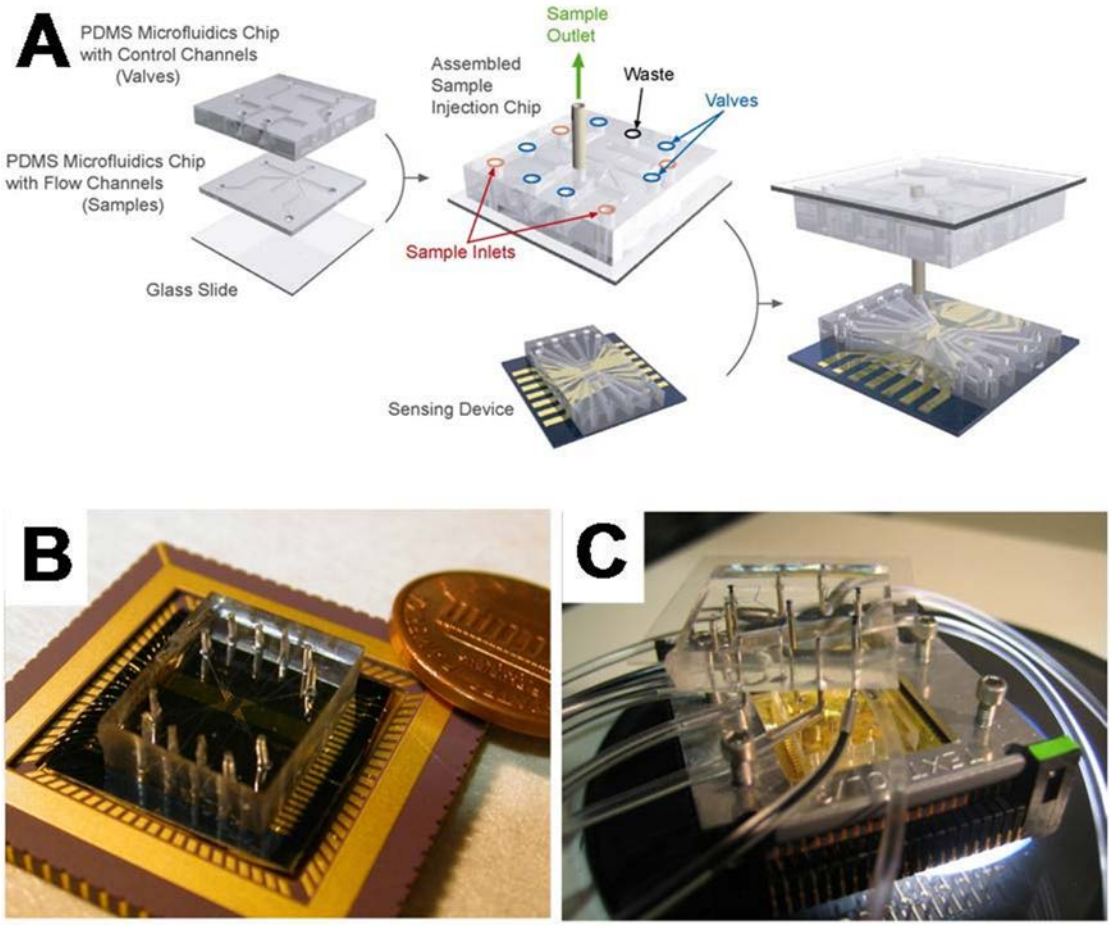

Figure 2.2 Sensing device and fluidics device for sample handling. (A) Fabrication and assembly of the two-layer PDMS chip for solution injection (top) with the sensing device composed of SOI wafer and a single-layer PDMS chip with six separate microchannels (bottom). (B) A photograph of a sensing device with PDMS chip containing six microchannels. The chip is fixed onto a chip carrier and the gold pads on the device are wirebonded to the gold pads of the chip carrier. (C) The sensing device with the PDMS chip on a chip carrier (B) is fixed into a chip carrier socket, and the PDMS chip for solution injection (A, top) is shown connected to one of the six microchannels of the sensing device, as outlined in schematic (A). The tubing with different solutions is feeding into the solution injection chip.

a control layer and a flow layer (Fig. 2.2A). For the fabrication of the flow layer, mixed PDMS was spin coated on a photoresist mold at 2500 rpm for 50 sec and incompletely cured at 80°C for 30 min. The control layer was fabricated by applying mixed PDMS over a photoresist mold directly and incompletely curing at 80°C, followed by the puncturing of

holes for inlets and outlets. The two layers were aligned together and the inlets/outlets for the flow layer were created. After two hours at 80°C, the two-layer PDMS chip was bonded to a glass slide via an O_2 plasma treatment. By utilizing such sample injection chip, we were able to control the injection and solution changing processes without disturbing the measurement, while maintaining the sensing device in an electrically isolated chamber at all times. The valves of the sample injection chip were actuated with the Labview program by means of the BOB3 Microfluidic Valve Manifold Controller and solenoid cluster manifolds (Fluidigm, Inc.). By introducing a waste outlet into the sample injection chip, we were able to remove any bubbles arising from switching between different solutions, which also helped in maintaining a stable baseline reading.

2.2.2 Surface functionalization and characterization for DNA sensing and antibody-based protein sensing

Synthesis of *tert*-Butyl allylcarbamate. To a solution of allylamine (2.27 g, 39.8 mmol) in THF (20 ml) was added *N*,*N*-diisopropylethylamine (13 ml, 80.0 mmol) followed by di-*tert*-butyl dicarbonate (8.7 g, 39.9 mmol). After 1 hr, the organic solvent was evaporated under reduced pressure, and the residue was purified by silica gel chromatography (Hex : EtOAc = 9 : 1) to give 6.6 g (93%) of a product as a clear oil. ^{1}H NMR 300 MHz ($CDCl_3$) δ 5.82 (m, 1H), 5.12 (m, 2H), 3.74 (bm, 2H), 1.45 (s, 9H).

Surface Functionalization. The two procedures used to functionalize SiNWs with and without oxide layer are shown in Schemes 2.1 and 2.2, respectively. Both procedures resulted in an amine terminated organic monolayer atop SiNWs. For the oxide surface functionalization, cleaned SiNWs were treated with 2% (v/v) 3-

aminopropyldimethylethoxysilane (Gelest, Inc., Morrisville, PA) in toluene for 2 hr. The wafers were then rinsed in toluene and methanol and incubated at 100°C for 1 hr.

The procedure described previously [42, 48] was used to functionalize hydrogen-terminated SiNWs with *tert*-Butyl allylcarbamate (Scheme 2.2). SiNWs were immersed in 2% HF solution for 3 s, washed with Millipore water and blow dried under N_2 stream. The wafer was immediately placed in a custom-made quartz container which was then pumped down to ~ 2×10^{-5} Torr, followed by an argon purge. Under positive argon pressure, a mixture of 1:2 *tert*-Butyl allylcarbamate:methanol (v/v) was applied to the wafer, completely covering the SiNWs. The wafer was illuminated with UV (254 nm, 9 mW/cm^2 at 10 cm) for 3 h. SiNWs were then rinsed in methylene chloride and methanol. The deprotection of t-Boc amine was carried out in a solution of TFA in methanol (1:4 v/v) for 4 h, followed by extensive methanol washing. In the case of antibody attachment, the amine-terminated surfaces were reacted with water-soluble homobifunctional N-hydroxysuccinimide ester (NHS ester), followed by the introduction of 50 µg/ml of

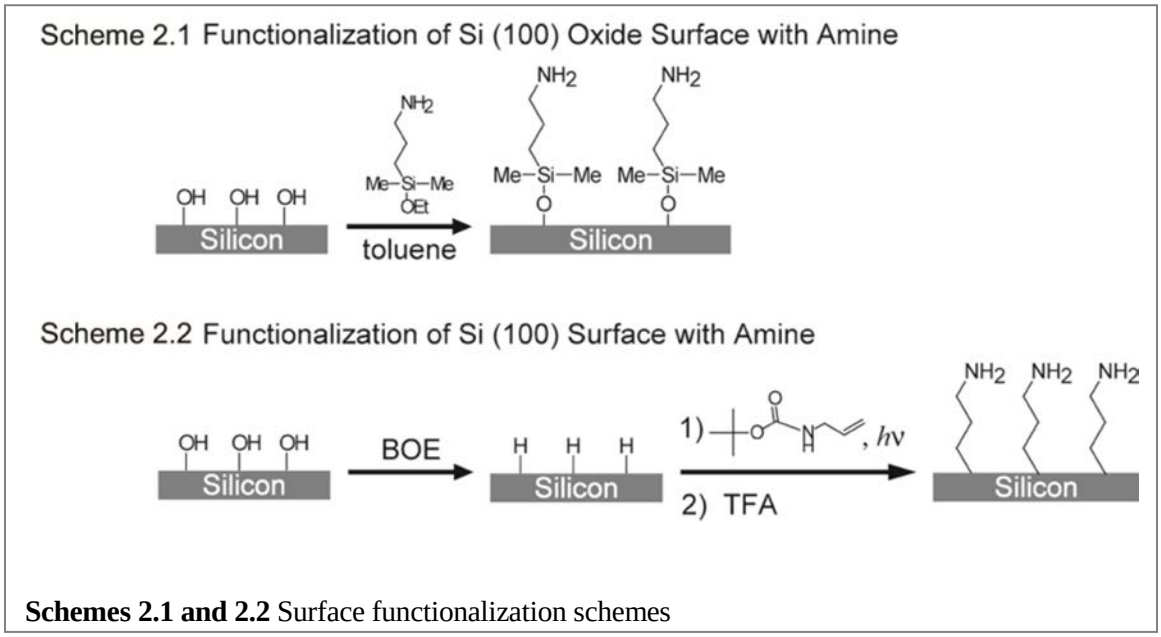

Schemes 2.1 and 2.2 Surface functionalization schemes

monoclonal anti-human IL-2 antibodies. The unreacted amines were quenched with ethanolamine (100 mM in 1×PBS).

X-ray photoelectron spectroscopy. X-ray photoelectron spectroscopy (XPS) was utilized to quantify the amount of oxide on Si(100) wafers after surface treatments outlined in Schemes 2.1 and 2.2. XPS was also used to follow the attachment of antibodies to silicon surfaces. All XPS measurements were performed in an ultrahigh vacuum chamber of an M-probe surface spectrometer that has been previously described.[53] Experiments were performed at room temperature, with 1486.6 eV X-ray from the Al Kα line and a 35° incident angle measured from the sample surface. ESCA-2000 software was used to collect the data. An approach described elsewhere [40, 53] was used to fit the Si 2p peaks and quantify the amount of surface SiO_x, assuming that the oxide layer was very thin. Any peak between 100 eV and 104 eV was assigned to Si^{+}-Si^{4+} and fitted as described in the literature.[54] SiO_x:Si 2p peak ratio was divided by a normalization constant of 0.17 for Si(100) surfaces.

Contact Angle Measurements. The sessile contact angle of water on the functionalized Si(100) surface was used to check the fidelity of surface chemistry as described in Schemes 2.1 and 2.2. Contact angle measurements were obtained with an NRL C.A. Goniometer Model #100-00 (Rame-Hart, Inc., Netcong, NJ) at room temperature. All measurements were repeated three times and averaged to obtain the contact angle θ for the surface.

2.2.3. Surface functionalization and characterization for peptide-based protein sensing

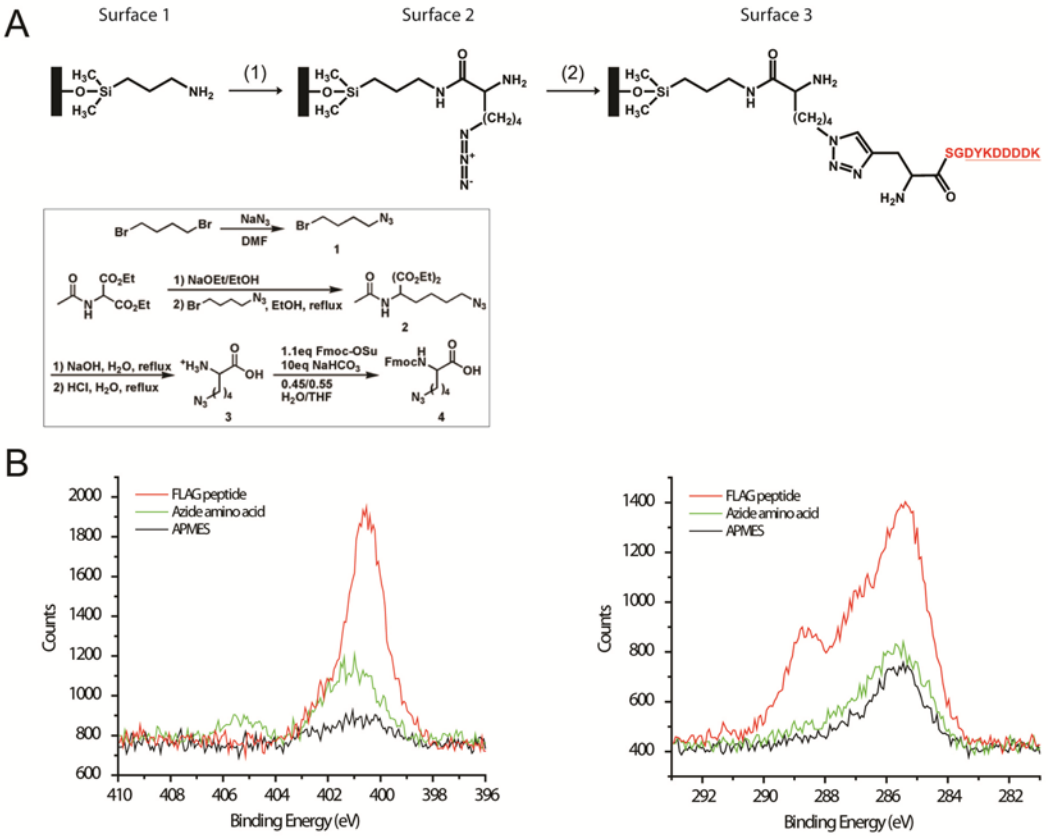

Figure 2.3 Surface treatment scheme for peptide functionalization on a Si (100) substrate and XPS data. (A) Amide coupling between a protected n-azidoalkyl amino acid and the APMES-treated surface, (1). Cu(I)-catalyzed click conjugation of the FLAG peptide (XSGDYKDDDDK) to the azide-modified surface, (2). The FLAG sequence contains an XSG spacer (X = L-propargylglycine). The spacer serves to introduce a terminal alkyne for the click reaction, and it enhances the accessibility of the FLAG binding motif presented by the surface. (Inset) Scheme for the four-step synthesis of the azide-containing unnatural amino acid used for surface modifications. (B) Monitoring the peptide functionalization by XPS. (Left) N 1s. (Right) C 1s

Peptide Synthesis and Purification. The FLAG peptide was synthesized on Fmoc-Rink Amide MBHA resin (0.67 mmol/g, Anaspec, San Jose, CA) using conventional solid-phase synthesis strategy with Fmoc protection chemistry**.** To prepare the peptide for click conjugation, a terminal alkyne was introduced by adding Fmoc-L-propargylglycine (Chem-Impex International, Wood Dale, IL), X, to the N-terminus to yield the sequence

XSGDYKDDDDK. The FLAG sequence also contains an SG spacer, to enhance the accessibility of the FLAG binding motif. The deprotected FLAG peptide was purified by HPLC on a C18 reversed phase column (Varian Dynamax semi-preparative column, 25 cm × 2.15 cm). The column was eluted with 0.1% trifluoroacetic acid and a two-step linear gradient of acetonitrile/water (3/2), rising from 0–25% over 30 min and 25–100% over 30 min. The pure FLAG peptide eluted at 41 min. The purified peptide product was verified to have the correct molecular weight as determined by mass spectrometry.

Synthesis of Azide-Containing Unnatural Amino Acid. The azide-containing unnatural amino acid used for surface modifications is synthesized by the following four steps.

Azidobutylbromide (1). To a solution of 1,4-dibromobutane (123 mmol), sodium azide (61.5 mmol) was added. The reaction mixture was stirred overnight at 50 °C, washed with water and brine, and dried over $MgSO_4$. The organic layer was concentrated and purified by silica gel chromatography (100% Hex) to give a product (80%) as clear oil.

Diethyl 2-acetamido-2-(4-azidobutyl)malonate (2). To a solution of 0.598 g (0.026 mol) sodium metal in 25 ml absolute EtOH was added 5.65 g diethyl acetamidomalonate (0.026 mol), following previously described procedures.[55] The mixture was stirred for 30 min at room temperature. By dropwise addition, azidobutylbromide **1** (4.82 g, 0.027 mol) was added with stirring. The reaction mixture was stirred for 2 h at room temperature and for 6 h at reflux. After cooling and standing for 14 h, the reaction mixture was concentrated to dryness, and the residue was extracted with ether. The combined ether extracts were washed with water, sat. $NaHCO_3$, and water, and were dried over $MgSO_4$ and then

concentrated. Silica gel chromatography (Hex:EtOAc = 1:1) gave a product (63%) as a clear oil.

2-Azidobutyl Amino Acid (3). Following standard methods,[56] the diester **2** (2.8 mmol) in 25 ml of 10% NaOH solution was heated to reflux for 4 h. The solution was then neutralized with concentrated HCl and evaporated. The residue was dissolved in 25 ml of 1 M HCl and heated to reflux for 3 h. The solvent was reduced and extraction with MeOH afforded amino acid **3** as a foamy solid (85%).

Fmoc-2-Azidobutyl Amino Acid (4). The amino acid **3** (26.3 mmol) was dissolved in 0.45:0.55 H_2O/THF (150 ml), and $NaHCO_3$ (22.1 g, 263 mmol) was added, following published methods.[57] After the mixture was cooled to 0°C, Fmoc-OSu (9.7 g, 28.9 mmol) was added dropwise over 5 min. The reaction mixture was allowed to come to room temperature and stirred overnight. The THF was evaporated *in vacuo* and the aqueous residue was washed with ether (2 x 200 ml). The aqueous layer was collected, acidified with concentrated HCl to pH 2 and extracted with ethyl acetate (4 x 100 ml). The combined organic layers were washed with brine, dried over $MgSO_4$, filtered, and concentrated. The organic residue was purified by column chromatography (2% MeOH in dichloromethane) to give a foamy solid. After recrystallization from EtOAc/Hex, a pure white powder was obtained (25% yield).

Surface Treatment. The cleaned silicon (100) surface was treated with 2% (v/v) 3-aminopropyldimethylethoxysilane (Gelest, Inc., Morrisville, PA) in toluene for 2 h followed by rinsing with toluene and isopropanol (IPA). The wafer was then incubated at 120°C for 15 min (APMES-treated surface in Fig. 2.3A). The amine-terminated surface was converted into an azide-terminated one through the conjugation of the azide-containing

unnatural amino acid (synthesized following the scheme in Fig. 2.3A, inset). A solution of 20 mM azide-containing unnatural amino acid in DMF was prepared to contain 8 equiv HATU, 4 equiv HOAt, and 24 equiv DIEA (relative to the azide). This coupling solution was incubated with the surface for 2 h at room temperature, followed by rinsing with IPA and water. The N-terminal Fmoc protecting group was removed by treatment with 20% piperidine in DMF for 30 min. After cleaning the device with IPA and water, a PDMS chip with microfluidics channel was bonded to the device. The PDMS chip was fabricated by the soft lithography technique described by others.[51] The channel was 150 μm wide and 20 μm high. The Cu(I)-catalyzed click conjugation of the FLAG peptide (XSGDYKDDDDK) to the azide-modified surface was performed. 20 equiv $CuSO_4 \cdot 5H_2O$ and 40 equiv sodium ascorbate (relative to the peptide) were mixed with a solution of 1 mM FLAG peptide in water and incubated over the device for 12 h in the prepared solution. Unreacted peptides and catalysts were rinsed away by flowing water through the channels. The FLAG sequence contains an XSG spacer (X = L-propargylglycine). The spacer serves to introduce a terminal alkyne for the click reaction, and it enhances the accessibility of the FLAG binding motif presented by the surface.

X-Ray Photoelectron Spectroscopy. X-ray photoelectron spectroscopy (XPS) was utilized to evaluate the surfaces at each step of the functionalization on Si (100) wafers. All XPS measurements were performed in an ultra-high vacuum chamber of an M-probe surface spectrometer that has been previously described.[53] Monochromatic Al K□X-rays (1486.6 eV) were used to irradiate the sample incident at 35° from the surface. ESCA-2000 software was used to collect and analyze the data. To gain an overview of the species present in the sample, survey scans were run from 0 to 1000 binding eV (BeV). The Si 2p

(95.5–107.5 BeV), C 1s (281–293 BeV), and N 1s (396–410 BeV) regions were investigated in detail.

Contact Angle Measurements. The sessile contact angle of water on the functionalized Si(100) surface was used to check the fidelity of surface chemistry. Contact angle measurements were obtained with an NRL C.A. Goniometer Model #100-00 (Rame-Hart, Inc., Netcong, NJ) at room temperature. All measurements were repeated ten times and averaged to obtain the contact angle for the surface.

2.2.4 SPR and electronic measurements

Surface Plasmon Resonance (SPR). All SPR experiments were performed on the Biacore 3000 with carboxylic-acid-terminated Biacore CM5 chips. The active flow cells were first primed in 1×SSC (15 mM NaCitrate, 150 mM NaCl, pH 7.5). To generate an amine surface, the carboxylic acid groups were converted to succinimide esters by flowing EDC/NHS prior to exposure of a 1 mg/ml solution of polylysine (Sigma-Aldrich, St. Louis, MO). Single-stranded DNA (5'TGGACGCATTGCACAT3', Midland Certified, Ind., Midland, TX) was electrostatically absorbed unto the polylysine matrix. Complementary DNA was then immediately introduced and allowed to hybridize to the active surface. The flow cell was regenerated with two 1-min pulses of 50 mM NaOH, after which ssDNA was reabsorbed electrostatically before another cDNA pulse was introduced for hybridization. The antibodies in acetate buffer (pH 5.5) were attached directly immediately following the surface treatment with EDC/NHS, and the remaining esters were reacted with ethanolamine. The antigen was introduced at various concentrations in 1×PBS buffer at the flow rate of 30

μl/min. Between each addition, the surface was regenerated with glycine/HCl buffer (pH 3.0).

Electronic Measurements. The 4-point resistivity of silicon film as well as SiNW resistances and solution gating were measured with a Keithley 2400 Source Meter (Keithley Instruments, Inc., Cleveland, OH). The sensing experiments were performed with a SR830 DSP Lock-in Amplifier (Stanford Research Systems, Inc., Sunnyvale, CA). Fig. 2.4 shows the experimental setup for the electronic measurements. A 50 mVrms at 13 Hz voltage source (V_{SD}) was applied to one terminal of the nanowire, with the amplifier input operating in the current-measure mode. For the DNA sensing experiments, platinum wire was inserted into the microchannel and used as a solution gate, while it was kept at a ground potential throughout the real-time measurements to reduce the noise in the system (Fig. 2.1A). In the case of protein sensing, the handle of the wafer (backside Si) was held at a ground potential instead of the platinum electrode in solution. The devices were functionalized and assembled as described above. Single-stranded 10 μM DNA (same as in SPR experiments) in 1×SSC buffer was flowed through the microchannel for 1 hr and allowed to electrostatically adsorb to the amine-terminated surface of SiNWs. The non-bound DNA was washed thoroughly with 1×SSC buffer. Complementary DNA (5'ATGTGCAATGCGTCCA3', Midland Certified, Ind., Midland, TX) of varying concentrations in 1×SSC buffer was sequentially injected from the injection PDMS chip into the microchannel containing SiNWs at a flow rate of 2.0 μl/min as the resistance of the NWs was recorded in real time. Noncomplementary DNA (noncomp. DNA) (5'CATGCATGATGTCACG3') was used as a control. In general, a different SiNW sensor

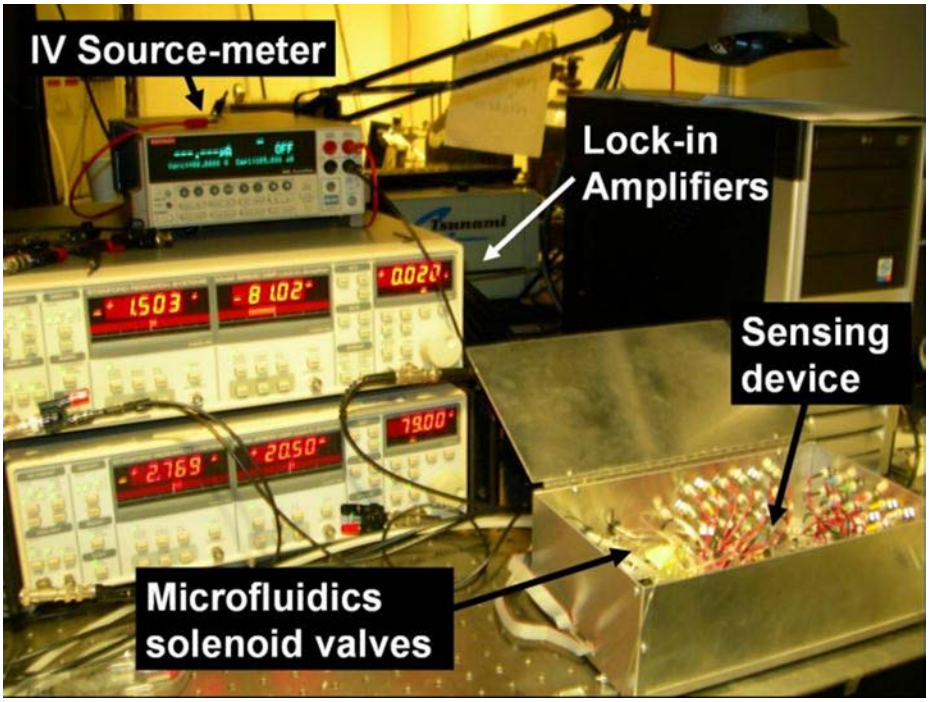

Figure 2.4 Experimental setup for biological sensing with silicon nanowires. The sensing devices (Figure 2.2C) are placed inside an electrically isolated box, which also contains solenoid manifolds that actuate microfluidic valves. The nanowire resistance is recorded in real-time with lock-in amplifiers.

was utilized for each of the measurements described here. Similar procedure was followed for protein sensing. The surface functionalized with capture antibodies was subjected to the 10 μM PBS solution containing various antigen concentrations (1 pM to 100 nM). After the introduction of a particular concentration, the surface was completely regenerated with 10 μM PBS, followed by the introduction of the next antigen concentration in the same microchannel.

2.3 Results and Discussion

2.3.1 DNA sensing

Surface Characterization. We used contact angle measurements to follow the functionalization processes of various surfaces. Table 2.1 presents the data for both Schemes 2.1 and 2.2. The procedure in Scheme 2.1 generates a large increase in contact angle. Similarly, large changes in contact angles are observed for photochemically treated Si surface before and after t-Boc deprotection. The resulting contact angle of ~ 60° is observed for surfaces prepared by Scheme 2.1 and 2.2, arguing for the existence of chemically similar, amine-terminated monolayers on these surfaces.

Quantifying the amount of oxide on the SOI NWs is extremely challenging. Therefore, we used Si(100) bulk surfaces to approximate the amount of surface oxide remaining after photochemical functionalization. Fig. 2.5A shows XPS scan in the Si/SiO_x region. The Si(100) surface with native oxide exhibited approximately 1.9 equivalent monolayers of

Table 2.1 Measured contact angles for various Si(100) surfaces

Si(100) surface	*contact angle*
With nonfunctionalized oxide	11 ± 1
Scheme 2.1: amine terminated	61 ± 1
Scheme 2.2: t-Boc protected	81 ± 1
Scheme 2.2: deprotected, amine terminated	60 ± 1

SiO_x. In contrast, the Si(100) surface treated according to Scheme 2.2 contained 0.08 equivalent monolayers of SiO_x prior to TFA deprotection and 0.3 monolayers of SiO_x after the deprotection step and a 10 h exposure to 1×SSC buffer. The roughness of a SiNW surface may cause a more extensive oxidation than the one observed on the bulk surface, but the data in Fig. 2.5A does demonstrate a significant reduction in oxide thickness after photochemical treatment. Furthermore, we used XPS to determine the presence of amine-terminated monolayer on bulk Si(100) surfaces post functionalization with two different

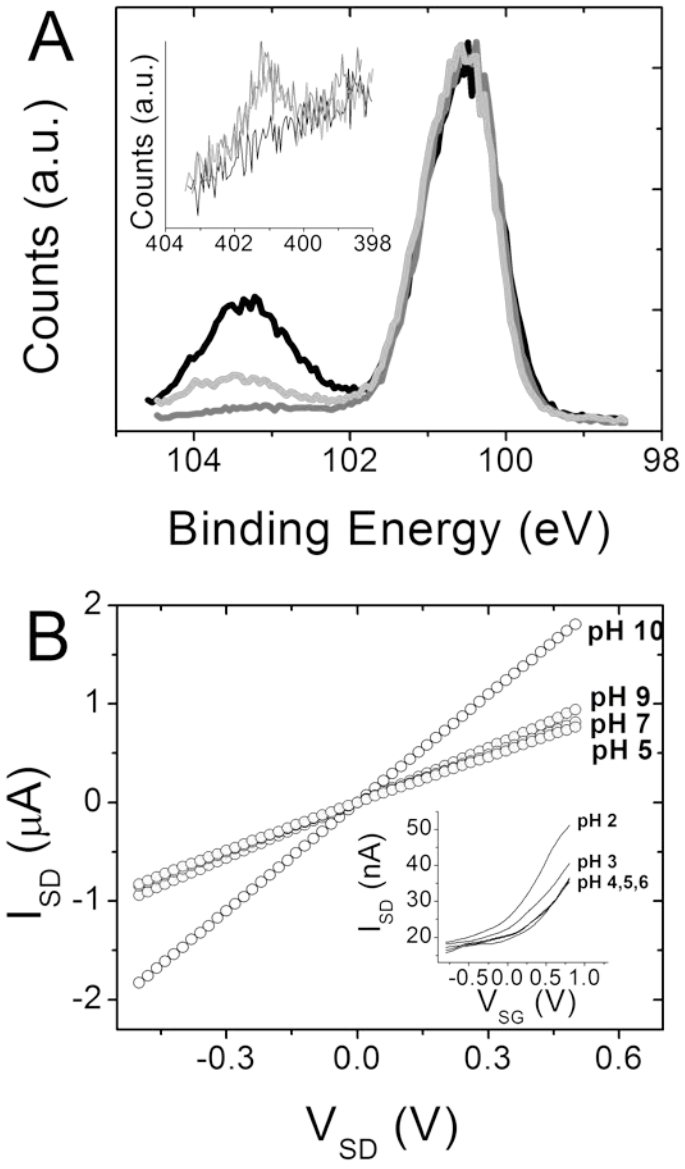

Figure 2.5 Surface analysis with XPS and SiNW response to pH. (A) XPS of Si 2p region of Si(100) surface functionalized as in Scheme 2.2 before (dark grey) and after (light grey) TFA deprotection and 10 hrs in 1×SSC buffer. Nonfunctionalized Si(100) surface with native oxide (black). Inset: N 1s region of nonfunctionalized Si(100) surface (black), Si(100) functionalized by Scheme 2.1 (light grey) and Scheme 2.2 (dark grey). (B) Current-voltage (IV) graphs of SiNWs functionalized by Scheme 2.1 in solutions of varying pH. Inset: Solution-gated (VSG) n-type hydroxyl terminated SiNW in solutions of varying pH

schemes. The Fig. 2.5A inset demonstrates the XPS scans of N 1s region. Nitrogen peak is clearly visible for surfaces functionalized by Schemes 2.1 and 2.2, while no peak is present for the nonfunctionalized Si.

Scheme 2.1 functionalized SiNWs demonstrate a sensitivity to pH which is different than for native oxide-passivated NWs.[13] The isoelectric point of silica is ~ 2,[58] implying that for hydroxyl-terminated, non-functionalized SiNWs at low pH, the SiOH groups are largely protonated. At high pH, negative charges on SiO^- should deplete carriers in the n-type SiNWs, causing a decrease in I_{DS} (Fig. 2.5B, inset). Above pH 4 the conductance is no longer modulated by increasing the pH, as most of the hydroxyl groups are deprotonated. When the surface is functionalized with amine (pK_a ~ 9–10), the opposite trend is expected. At low pH, the amine is protonated, causing carrier depletion or increased resistance in p-type SiNW. This trend is observed in Fig. 2.5B, where the sharpest transition in resistance occurs between pH 9 and 10. The observation of the correct pH effects on the resistance of the SiNWs serves as a confirmation of the presence of surface functional groups: amine in this case.

As shown in Fig. 2.6, oxide-covered SiNWs in 1×SSC buffer (0.165 M, pH 7.2) respond weakly to the applied solution gate voltage, V_{SG}, showing no significant on–off current transition between 0.8 and -0.8 volts. In contrast, directly passivated SiNWs (Scheme 2.2) exhibit on–off current ratios of ~ 10^2. Fig. 2.6 strongly suggests that directly passivated SiNWs exhibit an enhanced response to surface charges and should therefore serve as superior NW sensors compared with similarly functionalized, but oxide-passivated SiNWs.

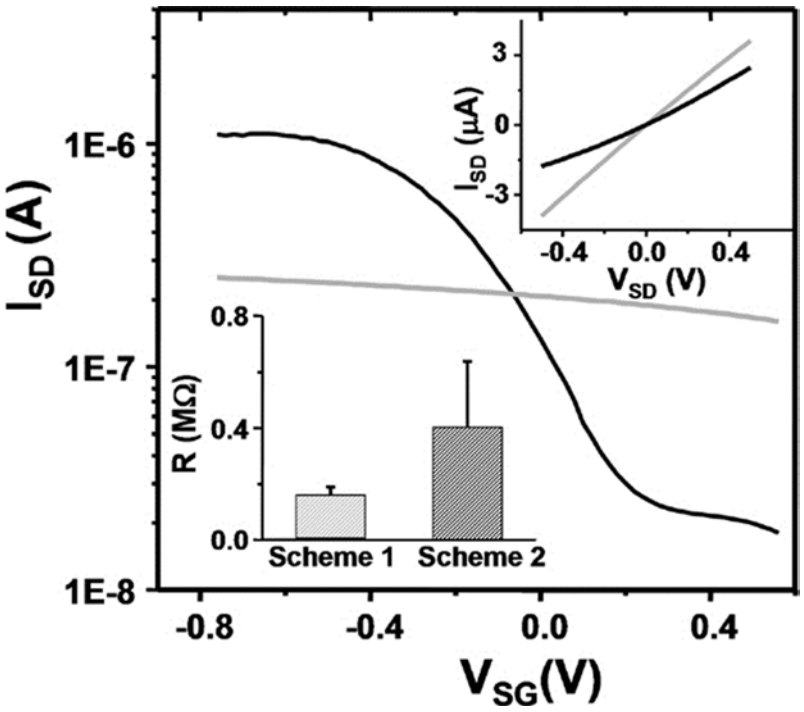

Figure 2.6 Solution gating of SiNWs functionalized by Scheme 2.1 (grey) and by Scheme 2.2 (black) (VSD was 50 mV). (Right inset) IV curves of SiNWs in air with (black) and without (grey) oxide. (Left inset) Resistances in air of SiNWs functionalized by Scheme 2.1 (left) and Scheme 2.2 (right)

The Scheme 2.2 procedure does involve an HF etch step, which can be potentially detrimental to the device conductance. We thus checked the conductivity of SiNWs before and after photochemical treatment. Lightly doped SiNWs provide for superior FET properties,[59] and, in fact, we have reported that lightly doped (10^{17} cm^{-3}) p- or n-type SiNWs are more sensitive biomolecular sensors than those reported here.[60] Our doping process preferentially dopes the top few nanometers of the SiNWs.[61] Thus, if the HF etching of the Si surface was extensive enough, we could expect an enhancement in SiNW current modulation by V_{SG} to be entirely due to the decrease in carrier concentration and not the removal of surface oxide. The Fig. 2.6 insets demonstrate that the NW resistance

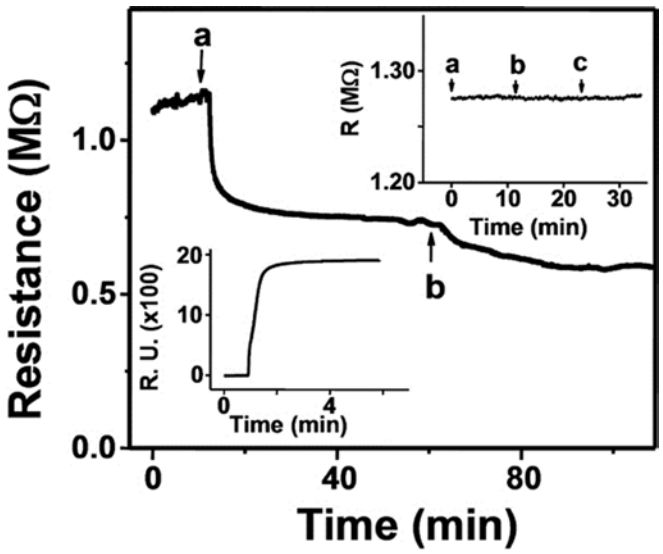

Figure 2.7 Real-time response of SiNWs functionalized as in Scheme 2.1 to the addition of (a) 10 μM ssDNA and (b) 100 nM complementary DNA. Right top inset: Real-time SiNW response to the sequential addition of (a) 0.165 M SSC, (b) 0.0165 M SSC, and (c) 0.00165 M SSC buffers. Left inset: SPR measurement demonstrating the addition of 10 μM ssDNA to poly-L-lysine coated CM5 sensor chip. VSD = 50 mV.

increased only, on average, by a factor of 2 following the HF treatment. This relatively negligible resistance increase indicates that the major reason that the SiNWs prepared by Scheme 2.2 exhibit an improved solution FET performance originates from the elimination of oxide via direct silicon passivation. This result is consistent with the recent demonstration that, for VLS-grown SiNWs, direct methylation of the SiNW surface leads to a 10^3–10^4-fold enhancement in the on–off conductance of the FETs made from those nanowires.[43]

Nanowire Sensing Measurements. Fig. 2.7 shows SiNW real-time detection of the electrostatic adsorption of 10 μM ssDNA, followed by the hybridization in 1×SSC buffer of 100 nM complementary DNA strand. As expected, the resistance of p-type SiNWs is decreased with the addition of negative surface charges. The metal contacts to NWs have

been covered with a Si_3N_4 layer, and there is no background conductance through the solution. We have observed an insignificant change in the resistance of the NWs upon switching from dry environment to buffer solution (data not shown). Moreover, as Fig. 2.7 (right inset) shows, changing the ionic strength of the solution does not affect the resistance. In addition, the automated solution injection removes any baseline shifts or transient changes in the resistance. SPR was also utilized in parallel to SiNWs in order to validate the surface chemistry and to obtain kinetic parameters such as k_{on}, k_{off}, and affinity constant K_A for this particular DNA pair. Poly-L-lysine was covalently attached to the SPR sensor chips, mimicking the amine-terminated monolayer of SiNWs. Fig. 2.7 (left inset) shows the SPR response to the electrostatic adsorption of a 10 μM primary DNA strand. The surface density of adsorbed DNA was estimated as 2.5×10^{13} cm^{-2}, using the conversion factor of 1000 RU = 100 ng cm^{-2} from the literature.[62] The surface density is approximately an order of magnitude higher than the average surface density of 10^{12} cm^{-2} obtained when localizing biotinylated DNA on a streptavidin-covered surface.[63] Such high surface density of primary DNA is expected because the poly-L-lysine-treated surface is positively charged. It is likely that the amine-terminated SiNW surface has less surface charge than the poly-L-lysine-covered surface and thus contains fewer sites for electrostatic adsorption of oligonucleotides.

Fig. 2.8 demonstrates real-time label-free detection of ssDNA by SiNWs and by SPR. In either case, the primary DNA strand was electrostatically immobilized on the sensor surface. Known DNA concentrations were injected after a stable reading with 1×SSC buffer was obtained and the flow was maintained throughout the experiment. Different concentrations were detected with different groups of SiNWs. We observed that the

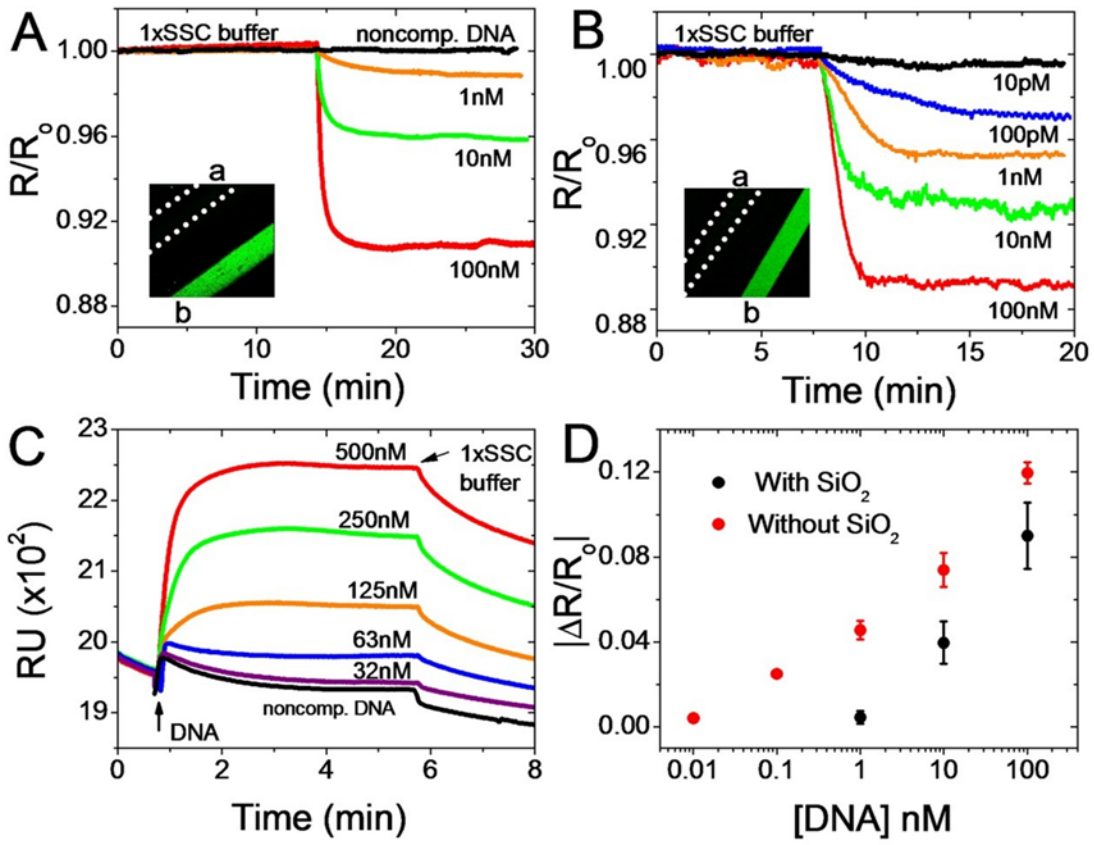

Figure 2.8 Concentration-dependent, real-time sensing of complementary DNA by SiNWs and by SPR in 0.165 M electrolyte. (A) Real-time responses of SiNWs that were surface functionalized according to Scheme 2.1 and coated with electrostatically adsorbed primary DNA. The black trace represents exposure of the SiNW sensors to 100 nM non-complementary ssDNA. Each curve represents measurements from a different set of NWs. Inset: Fluorescence image of Si(100) surface (with overlaying PDMS microfluidics chip) treated as in Scheme 2.1 followed by 10 μM primary DNA addition and addition of (microchannel a) 100 nM noncomplementary fluorescent DNA and (microchannel b) 100 nM complemenatary fluorescent DNA. PDMS chip was removed before the image was collected. (B) As in (A), except the SiNWs were functionalized according to Scheme 2.2. Inset: Same as in A inset, but Si(100) surface was treated as in Scheme 2.2. (C) SPR measurement of the hybridization of complementary DNA to electrostatically adsorbed primary DNA on a poly-L-lysine surface. (D) Normalized SiNW responses for Scheme 2.1 (black dots) and Scheme 2.2 (red dots) surface preparations, as a function of the log of DNA concentration. For all measurements, VSD = 50 mV.

hybridization on SiNWs is essentially irreversible on the relevant time scales when the analyte DNA was being washed away with the buffer solution. Such behavior is in contrast to SPR measurements, where the slow reversal of hybridization was observed (Fig. 2.8C). The performance of the NWs surface functionalized according to Scheme 2.1 (Fig. 2.8A) was compared to SiNW sensors prepared according to Scheme 2.2 (Fig. 2.8B). The SPR experiments, although carried out on Au substrates, also utilized primary ssDNA that was electrostatically adsorbed onto an amine-terminated surface. The intention here was to find experimental conditions that could serve to validate the NW experiments by obtaining kinetic parameters for these particular DNA strands under specific experimental conditions. Control experiments with non-complementary DNA yielded no response for either SiNWs or SPR measurements (black traces of Figs. 2.8A and 2.8C). These negative controls were also independently validated via fluorescent detection in microfluidic channels on two different (Schemes 2.1 and 2.2) Si surfaces (Figs. 2.8A and 2.8B, insets). Fig. 2.8D demonstrates that the NW response ($\Delta R/R_o$) varies as log[DNA]. Such a logarithmic dependence has been previously reported.[21] As demonstrated in Fig. 2.8D, the dynamic range of SiNWs is increased by 100 after the removal of oxide and UV-initiated chemical passivation; the limit of detection (LOD) increased from 1 nM to 10 pM.

Nanowires as Quantitative Biomolecular Sensors. SiNW sensors can potentially be utilized to quantitate analyte concentration and binding constants. In order to explore this possibility, the SiNW sensing response must be compared with other label-free, real-time methods such as SPR. It is also critical to design experimental parameters for both sensing modalities that are as similar as possible, as was described above. In this section, we first discuss the use of electrostatically adsorbed primary DNA for detecting complementary

DNA analyte. We then discuss the development of a self-consistent model that allows for the direct comparison of SPR measurements with nanowire sensing data. Finally, we test that model by utilizing the nanowire sensing data to calculate 16-mer DNA binding constants and analyte concentrations.

Previous studies have demonstrated that the Langmuir model can be applied for parameterization of the hybridization processes of short oligonucleotides.[22, 63] We used the Langmuir model to calculate kinetic parameters from the SPR hybridization measurements (Fig. 2.8C) and obtained $k_{on}=1\times10^{5}$, $k_{off}=2\times10^{-2}$, $K_A=5\times10^{6}$ (Table 2.2). This K_A value is between 10 and 100 times smaller than that reported for similar length DNA measured with a quartz crystal microbalance, SPR,[22] and surface plasmon diffraction sensors (SPDS).[63] The average primary DNA surface coverage in those studies was ~ 5×10^{12} molecules/cm^2. As stated above, the electrostatically adsorbed DNA coverage in our SPR experiments was approximately 10 times higher, at 2.5×10^{13} cm^{-2}. This difference in coverage likely arises from the differing methods of DNA immobilization; while in our system the DNA is electrostatically adsorbed, other studies utilized a streptavidin-biotinylated DNA linkage for surface immobilization.[22, 63] High surface coverage of primary DNA significantly reduces the efficiency of hybridization.[63, 64] In addition, the hybridized duplex of electrostatically adsorbed and covalently bound DNA may be structurally and energetically different. It has been proposed that a preferred structural isomer of an oligonucleotide pair on a positively charged surface is a highly asymmetrical and unwound duplex.[65] We believe that such non-helical nature of DNA duplex, together with steric effects of highly packed surface play major roles in the reduced affinity for the 15mer pair used in this study.

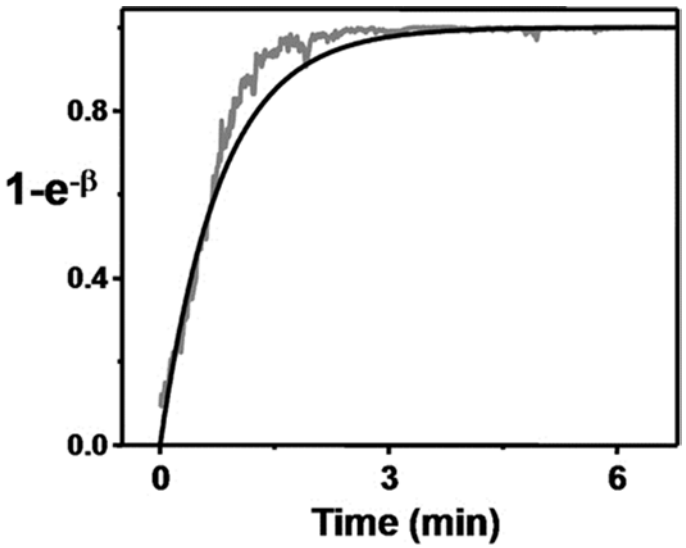

Figure 2.9 Comparison of SPR-derived hybridization kinetic parameters with NW sensing data. The black line represents eq. 5 plotted using k_{on} and k_{off} obtained from SPR measurements, $\beta=(k_{on}C+k_{off})t$. The grey trace is obtained from SiNW resistance vs. time data, $\beta = \frac{\Delta R}{R_{\max} - R}$. C = 10 nM.

We now turn toward developing a model for using SiNW sensors to quantitate complementary DNA pair-binding constants, and, if those numbers are known, to determine the solution concentration of the analyte. A discussion of the kinetics of a surface binding assay, as measured within flowing microfluidics environments, is required. Zimmermann and coworkers modeled the kinetics of surface immunoassays in microfluidics environments.[66] Their model was based on four differential equations: the two Navier-Stokes partial differential equations, the Convection-Diffusion equation, and the ordinary differential equation resulting from the Langmuir binding model (i.e., the binding/hybridization equilibrium). A key result was that in the limit of high analyte flow speeds (> 0.5 mm/sec) (which is the case for all the experiments here) the amount of

analyte that is captured and ready for detection can be described by the ordinary differential equation resulting from the Langmuir binding model:

$$\frac{d\Theta_t}{dt} = k_{on}C\left(\Theta_{\max} - \Theta_t\right) - k_{off}\Theta_t \ . \qquad (2.1)$$

Here, Θ_t = surface density of bound analyte molecules; k_{on} = rate constant for association; k_{off} = rate constant for dissociation; C = solution concentration of analyte (a constant under flowing conditions); $\Theta_{\max}$ = maximum number of binding sites available per surface area. Eq. 2.1 can be solved analytically:

$$\Theta_t = \frac{k_{on}\Theta_{\max}C}{k_{on}C + k_{off}}\left(1 - e^{-\left(k_{on}C + k_{off}\right)t}\right) \qquad (2.2)$$

.

The challenge is to translate from the resistance change of a SiNW sensor to the analyte concentration, C. However, the exact relationship between a measured resistance change and the surface density of bound analyte molecules is not intuitively clear. Here we attempt to determine the nature of that relationship.

We demonstrated above (Fig. 2.8D) that the cumulative change in SiNW sensor resistance arising from the binding of a charged analyte (ssDNA) at a concentration-dependent saturation was linearly proportional to the log[DNA], similar to what has been reported for VLS SiNW detection of prostate-specific antigen (PSA).[21] In mathematical terms, this means that as we approach saturation for a given concentration:

$$\frac{\Delta R}{R_0} = \alpha \ln C \qquad (2.3)$$

where α is a constant, $\Delta R = R - R_o$, R is resistance at time t, and R_o is the resistance at t = 0. At saturation levels eq. 2.2 reduces to $\Theta_t = \frac{k_{on}\Theta_{\max}C}{k_{on}C + k_{off}} = \frac{K_A\Theta_{\max}C}{K_AC + 1}$ (where the binding

affinity $K_A = \frac{k_{on}}{k_{off}}$). In the limit where $K_A C << 1$ (which is usually the case with values of $C \leq 10^{-9}$ and values of $K_A < 10^8$), this reduces to $\Theta_t = K_A \Theta_{\max} C$. Therefore, at saturation, and with $K_A C << 1$, Θ_t scales linearly with C. From our previous discussion, this implies that at saturation $\frac{\Delta R}{R_0}$ scales logarithmically with Θ_t (or equivalently that Θ_t is an exponential function of $\frac{\Delta R}{R_0}$ at saturation). In estimating the relationship between resistance changes at all times (not just at saturation) and the surface density of bound analyte molecules at all corresponding times, we start by assuming the same functional relationship that we experimentally observe at saturation. We also impose two boundary conditions. (1) When the measured resistance reaches its saturation level we would expect the maximum number of binding events to have taken place and for that number to be consistent with the prediction from the Langmuir binding model (eq. 2.2). (2) When the measured resistance is unchanged from its starting level we expect zero binding events (again consistent with the Langmuir model at time = 0). Based on these assumptions and boundary conditions we can thus estimate that the surface density of bound analyte molecules as a function of resistance change has the form:

$$\Theta_t = \frac{k_{on}\Theta_{\max} C}{k_{on} C + k_{off}} \left(1 - e^{\frac{-\Delta R}{R_{\max} - R}} \right) \text{; } (R_{max} = \text{R at saturation}). \qquad (2.4)$$

The validity of eq. 2.4 can be tested by considering the following expression that is derived from eq. 2.4 and comparing it to the same expression derived from eq. 2.2:

$$\Theta_t \Big/ \frac{k_{on}\Theta_{\max}C}{k_{on}C + k_{off}} = [1 - e^{\frac{-\Delta R}{R_{\max} - R}}] = [1 - e^{-(k_{on}C + k_{off})t}] \qquad (2.5)$$

.

Note that eq. 2.5 is expressing the fraction of bound analyte molecules at time t relative to the level at saturation in terms of ΔR (first term in brackets) and in terms of binding constants (second term in brackets). Time appears explicitly in the second term in brackets, while it is implicit in the first term in brackets (i.e., at a given time t there is a given R and ΔR). If we plot the first term in brackets in eq. 2.5 (the term containing ΔR) against the second term in brackets (using k_{on} and k_{off} values from an SPR analysis), we find that the two curves are similar (Fig. 2.9).

A second test of eq. 2.4 is to utilize it to extract binding kinetics. As we can infer from eq. 2.5, if eq. 2.4 is equivalent to the Langmuir binding model (eq. 2.2), then:

$$\frac{\Delta R}{R_{\max} - R} = (k_{on}C + k_{off})t \qquad (2.6)$$

.

We can thus extract k_{on} and k_{off} values from measured resistance data. We can select R vs. time traces at any two concentration values. Taking R and ΔR at an arbitrary point in time and noting $R_{\max}$ (the resistance at saturation), we have two equations (one for each concentration C) and two unknowns. We thus solve for k_{on} and k_{off} and compare directly with kinetic parameters obtained from SPR experiments. The k_{on}, k_{off}, and K_A values are summarized in Table 2.2. The k_{on} constants determined from the SiNW experiments are 3–5 times larger than k_{on} obtained with SPR experiments. The nanowire-measured k_{off} values, however, are consistently quite close to those measured with SPR. As stated above, the variation in k_{on} values may be a reflection of steric affects that arise from the unusually high surface density of primary DNA adsorbed onto the poly-L-lysine surfaces that were

	SiNWs–concentration pair:			SPR (this work) (poly-L-lysine surface, 16-mer DNA)	SPDS (ref. 63) (avidin-biotin linkage, 15-mer DNA)
	10 nM 100 nM	1 nM 100 nM	1 nM 10 nM		
k_{on} ($M^{-1} s^{-1}$)	$3.5(3.4) \times 10^5$	$4.2(2.4) \times 10^5$	$6.2(9.6) \times 10^5$	1.01×10^5	6.58×10^4
Δk_{off} (s^{-1})	$3.1\ (0.5) \times 10^{-2}$	$2.4\ (0.8) \times 10^{-2}$	$2.4\ (0.9) \times 10^{-2}$	2.01×10^{-2}	1.32×10^{-4}
K_A (M^{-1})	1.1×10^7	1.8×10^7	2.6×10^7	5.02×10^6	4.98×10^8
[DNA]	100 nM (actual); 68(52) nM calculated 10 nM (actual); 14(9) nM calculated				

Table 2.2 Kinetic parameters estimated from SiNW biosensors for the hybridization of 16-mer DNA and corresponding comparisons with analogous SPR and SPDS (surface plasmon diffraction sensor).[63] The calculated concentrations (bottom row) were estimated with eq. 6, by using the pair of SiNW measurements that did not include the concentration to be determined. For example, the 1 nM and 100 nM measurements were used to determine the concentration at 10 nM. Standard deviations are given in parentheses.

used for the SPR experiments.[63, 64]

Further work has to be done to ground this translation from nanowire-resistant readings to the Langmuir binding model (or equivalently from resistance readings to number of bound analyte molecules) on firm theoretical grounds. It is encouraging, however, that with our resistance data we can extract useful binding kinetics. The most useful application of our model would be in extracting otherwise unknown concentration values once k_{on} and k_{off} values are known. As demonstrated here and elsewhere, SiNW sensors can be used for label-free biomolecule detection at concentrations significantly below the limits of detection for SPR. Thus, the potential for SiNW sensors to quantitate analyte concentrations when the concentrations are below 10 nM represents a nontrivial application. The consistency of the SiNW measurements that is reflected in the Table 2.2 values is worth noting, especially since each measurement was carried out using a different SiNW

sensor. This provides validation that the nanofabrication techniques that were utilized to prepare the NW sensing devices are highly reproducible.

2.3.2 Protein sensing with antibodies

Robust label-free detection of proteins below the concentration of ~ 10 pM is of considerable importance in rapid clinical evaluation, cancer marker detection, disease staging, etc. The real-time nature of electronic label-free detection also offers additional

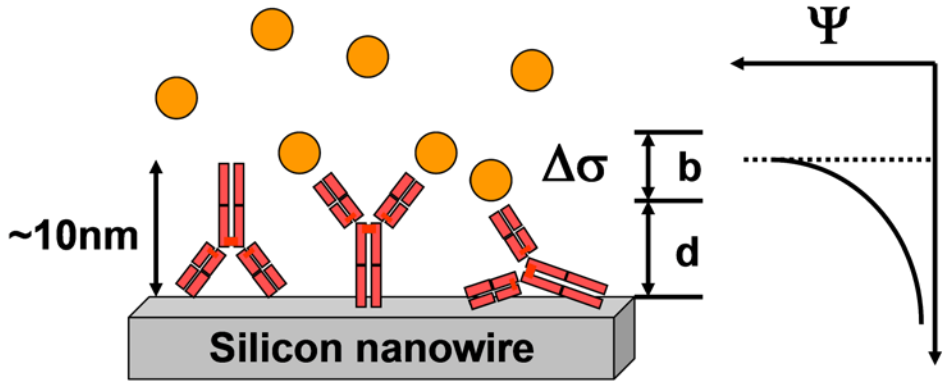

Scheme 2.3 The binding of proteins to antibodies at a distance ~ 10 nm from the surface of silicon nanowires results in an approximately homogeneous change in charge density, Δσ, which is smeared over a distance b. The accompanying change in chemical potential, Ψ, drops off exponentially, with a characteristic Debye length, 1/κ.

benefits such as characterization of new affinity probes, drug screening, and could, therefore, be potentially useful in basic research as well as in clinical practice. For these reasons, we have extended the above study to the detection of proteins. Such endeavor, however, faces a fundamental challenge, owing to the significant charge screening in the solution of high ionic strength. The extent of such screening may be characterized by the Debye length, 1/κ,[20] which describes a distance from a point charge at which the potential

due to that charge drops off to ~ e^{-1} of its value. Scheme 2.3 demonstrates the relevance of Debye screening to the electrical detection of biomolecules in solution. Here, we assume that the antibodies, which serve as capture probes for proteins, are approximately 10 nm long, and are randomly oriented on the surface of the nanowire. The change in charge density, $\Delta\sigma$, due to the equilibrium binding of proteins is smeared over a distance b, which is a distance d away from the NW surface. The change in chemical potential per area at the surface of the nanowire may be described by the Debye-Hückel equation,[18, 20]

$$\Delta\Psi = \frac{\Delta\sigma}{b}\frac{\left[e^{-\kappa d} - e^{-\kappa(d+b)}\right]}{\varepsilon_0\varepsilon_w\kappa^2} \qquad (2.7)$$

where ε_0 is the dielectric constant, ε_w is the permittivity of water and κ^{-1} is the Debye screening length. As is readily noticeable from eq. 2.7, the larger the $1/\kappa$ (smaller κ), the more pronounced will be the surface potential change for a given change in the charge density. Surface potential and the distance from the surface at which the binding takes place are intimately coupled. If the screening length is much smaller than d, $\kappa^{-1} << d$, then the potential due to protein binding will be completely screened from the surface of the nanowire. Therefore, the condition $\kappa^{-1} \geq d$ must be met in order to detect charged species in the solution a distance d away from the surface. In the case of DNA sensing (Section 2.3.1), the capture probe single-stranded DNA was electrostatically adsorbed on the NW surface, and the hybridization was taking place very close, ~ 1 nm from the surface, allowing us to carry out sensing in high ionic strength conditions of 0.165 M. The antibodies, however, are fairly large biomolecules (Scheme 2.3). At 25°C the Debye length of aqueous solution is[20]

$$\frac{1}{\kappa} = \frac{0.304}{\sqrt{[NaCl]}} nm \qquad \textbf{(2.8)}$$

for 1:1 electrolytes such as NaCl.

As Table 2.3 demonstrates, the size of the antibodies dictates the ionic strength of the solution in which the electronic detection may take place. This is a serious limitation if the physiological medium such as serium (0.14 M) must be used to detect low abundance proteins, without the possibility of appropriate dilutions. To circumvent this problem, new high-affinity probes, such as aptamers, small molecules, and short peptides, must be developed, all of which are significantly smaller than the antibodies.

[NaCl]	**1/κ**
100 mM	1 nm
1 mM	10 nm
10 μM	100 nm

Table 2.3 Debye length at different salt concentrations

SiNW surfaces for protein sensing were functionalized in a similar manner to the experiments with DNA. Native oxide of silicon was functionalized with an amine-terminating monolayer. A bifunctional crosslinker, with an NHS ester on either end, was coupled to the primary amines on the surface, followed by the coupling of antibodies to the other end of the linker. This chemistry may potentially involve any of the primary amines of the antibody, and, therefore, probably results in a random orientation of the antibodies on the surface (Scheme 2.3). Since the surface area of a nanowire is rather small, ~ 10^{-13} m^2, this may result in the broadening of the distribution of the responses from the identical

nanowires. Measuring the response of a larger array of nanowires, therefore, may lead to a smaller variance in the response.

XPS scans of the carbon 1s region from the silicon surface treated as described above are presented in Fig. 2.10. Clear emergence of the C=O and C-O/C-N bonds is visible, suggesting that the antibodies are successfully attached to the surface. The doping level was chosen as the one which reproducibly yields wires with resistances of ~ 1 MΩ, ohmic contacts, and good solution transconductance behavior (Fig. 2.11A). Wires with higher doping are not as sensitive to proteins and those with lower doping yield fewer functional devices.

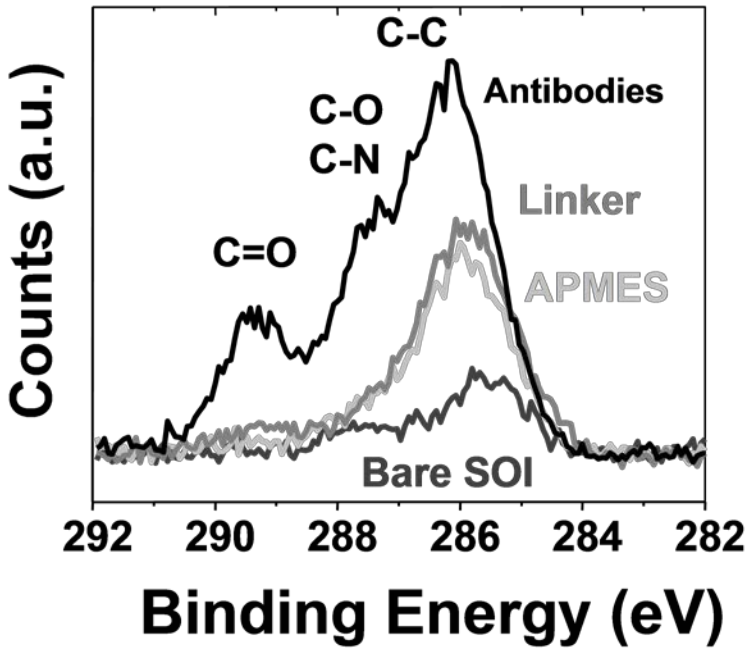

Figure 2.10 XPS of carbon 1s region, followed through the process of nanowire functionalization with antibodies. Starting with bare silicon-on-insulator (SOI) substrate (dark grey), the wafer is functionalized with 3-aminopropyldimethylethoxysilane (APMES) as described in the Experimental Methods Section (light grey). Bifunctional cross-linker (NHS ester) is then attached to the surface amines (grey), followed by the covalent attachment of antibodies (black).

The attachment of antibodies was further verified by monitoring the resistance of the nanowires during the functionalization process. Fig. 2.11B shows IV curves of the nanowires in air, in solution, and after the attachment of the antibodies. The resistance of

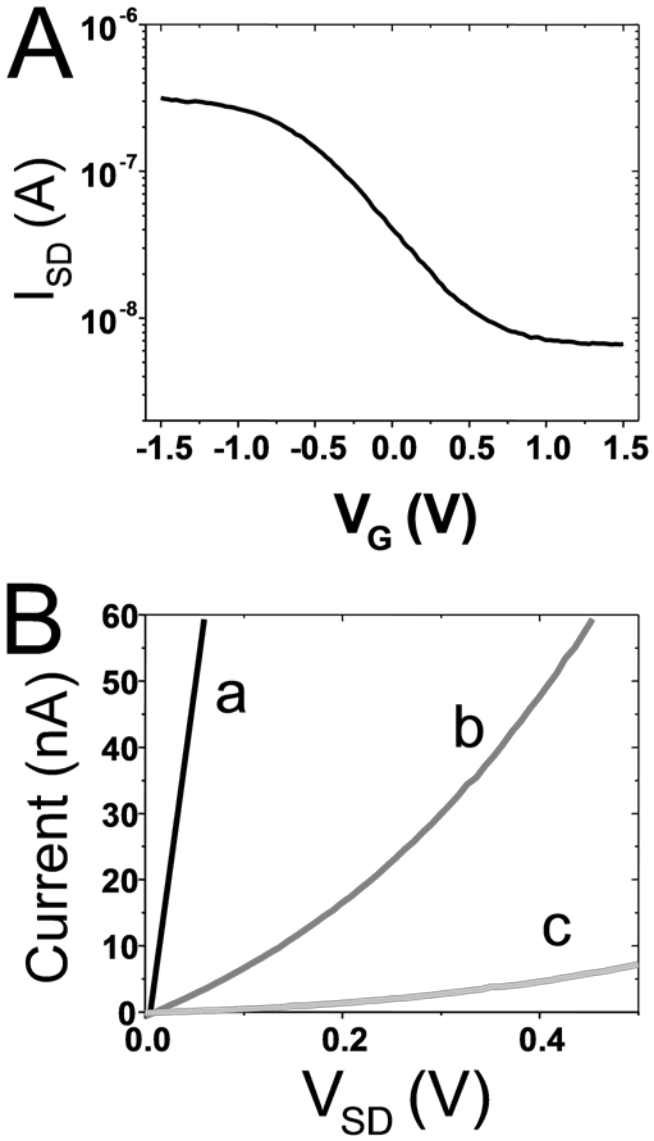

Figure 2.11 Solution gating responses. (A) SiNW (~ 10^{18} cm^{-3}) response to the application of solution gate voltage in 10 μM PBS solution. (B) Current-voltage traces of SiNW (~ 10^{18} cm^{-3}) (a) with surface amine in air, (b) with surface amine in10μM PBS solution, (c) after antibody attachment in 10 μM PBS solution

the amine-terminated nanowires drops significantly after immersion in solution and yet further after the attachment of the antibodies. The pH of the 10 μM PBS is approximately 6.0, which may account for the increase in the resistance in the solution. It is also possible that pH 6.0 is below the isoelectric point of the particular antibody used here, and the excess positive charges on the antibody surface lead to the further increase in the resistance.

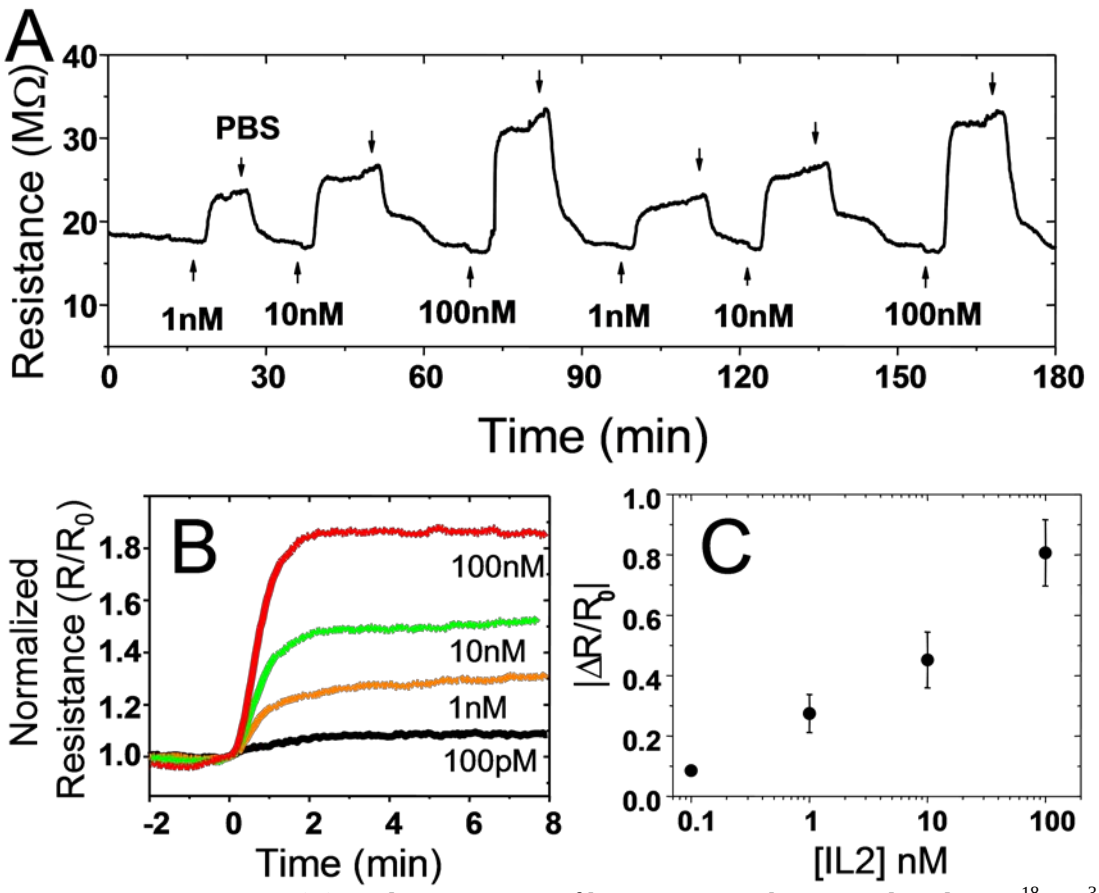

Figure 2.12 IL-2 sensing. (A) Real-time sensing of human IL-2 with SiNWs doped at 10^{-18} cm^{-3}. The nanowires were functionalized with 3-aminopropyltriethoxysilane (APTES), followed by the attachment of anti-human IL-2 antibodies. Human IL-2 in 1.5 μM PBS at different concentrations (1 nM, 10 nM, and 100 nM) was introduced, each time followed by the removal of bound IL-2 with 1.5 μM PBS. (B) Normalized resistance of nanowires (R_0 is an initial resistance) as a function of time and IL-2 concentration. (C) Normalized change in resistance $\{\Delta R/R_0=(R_{sat}-R_0)/R_0\}$ as a function of protein concentration

Real-time detection of proteins with SiNWs is demonstrated in Figs. 2.13 and 2.15. In each case, the same microchannel (the same SiNWs) was used for introducing antigen at various concentrations. After the saturation of the signal, phosphate buffer was used to remove bound human interleukin-2 (IL-2). This process was repeated several times with different IL-2 concentrations, and as Figs. 2.12A and 2.14A demonstrate, the antigen-antibody binding is fully reversible. SiNWs can, therefore, similarly to the SPR chip, be reused multiple times for protein detection. The data in Fig. 2.12 was collected in 1.5 μM PBS using the chip which was functionalized with 3-aminopropyltriethoxysilane (APTES).

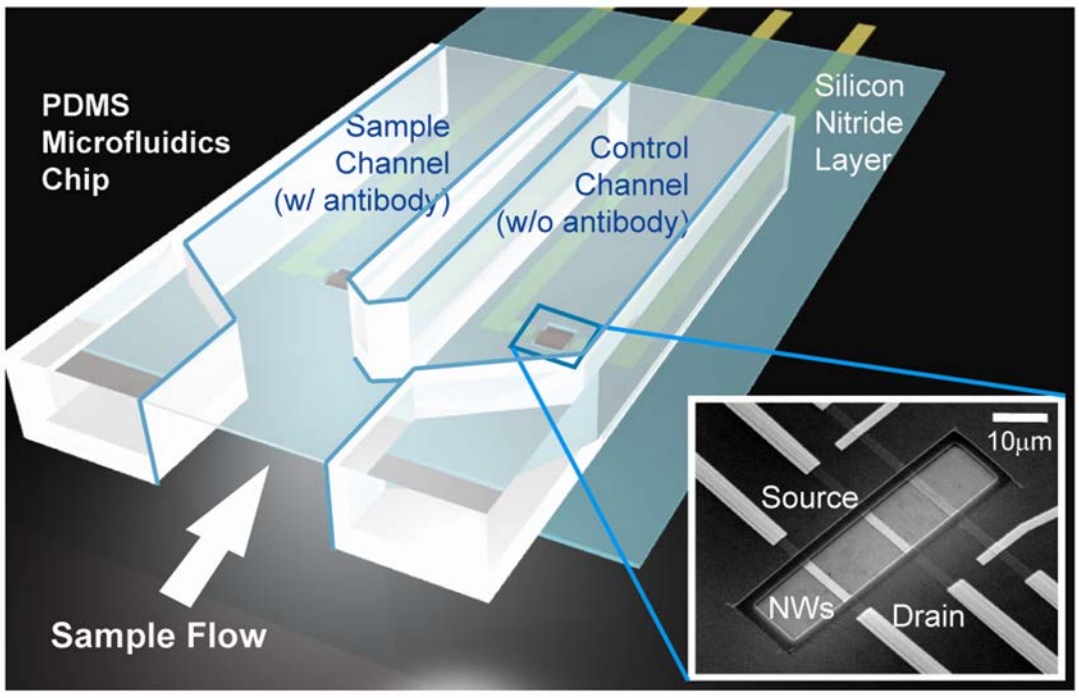

Figure 2.13 Schematic of the microfluidic PDMS chip overlaying a nanowire sensor device for differential measurements. A single microchannel bifurcates into two channels, each delivering solution to a separate sensor region with SiNWs (inset). One of the two sensor regions is functionalized with antibodies (left channel), while the other serves as a reference (right channel), accounting for the signal due to non-specific binding. The analyte solution is flown over both regions simultaneously (arrow), and the real-time resistance of the two regions is subtracted.

APTES forms multilayers on the surface due to intermolecular polymerization. After the data in Fig. 2.12 was collected, the chip was cleaned in organic solvents and briefly in O_2 plasma. The surface of the SiNWs was then functionalized with 3-aminopropyldimethylethoxysilane (APMES), which forms a monolayer on silicon oxide surface. Subsequent protein sensing was carried out in 10 μM PBS. For this time, devices were modified (original devices as in Fig. 2.1) to include a control channel for each measurement (Fig. 2.13), which contained nonfunctionalized SiNWs. It is expected that such bare SiNWs provide a measure of nonspecific protein binding to the surface; therefore, a differential measurement taking biofouling and random drift into account is more accurate.

As evident from comparing Figs. 2.12 and 2.14, while the same SiNW device was used for protein sensing, the changes in resistance corresponding to the same concentrations of IL-2 are markedly different. The reason for this difference is difficult to pinpoint exactly. In Fig. 2.12, the functionalization with APTES may have resulted in a higher density of surface amines, which translated to a higher surface density of anti-IL-2 antibodies, and, therefore, to a larger saturation signal. Also, longer Debye screening length, corresponding to the detection in 1.5 μM PBS (Fig. 2.12), vs. 10 μM PBS (Fig. 2.14), may have also contributed to higher signals. Finally, O_2 treatment may have oxidized the surface, leading to a drop in sensitivity. Regardless of the exact reason, it is evident that the sensing devices may be reused multiple times for protein detection. Fig. 2.14 demonstrates that the increase in resistance is specific to antibody-IL-2 binding. When the antibodies are absent from the SiNW surface, no changes in the resistance are observed, meaning that the nonspecific binding of the antigen is below the detection threshold. In addition, the response of the

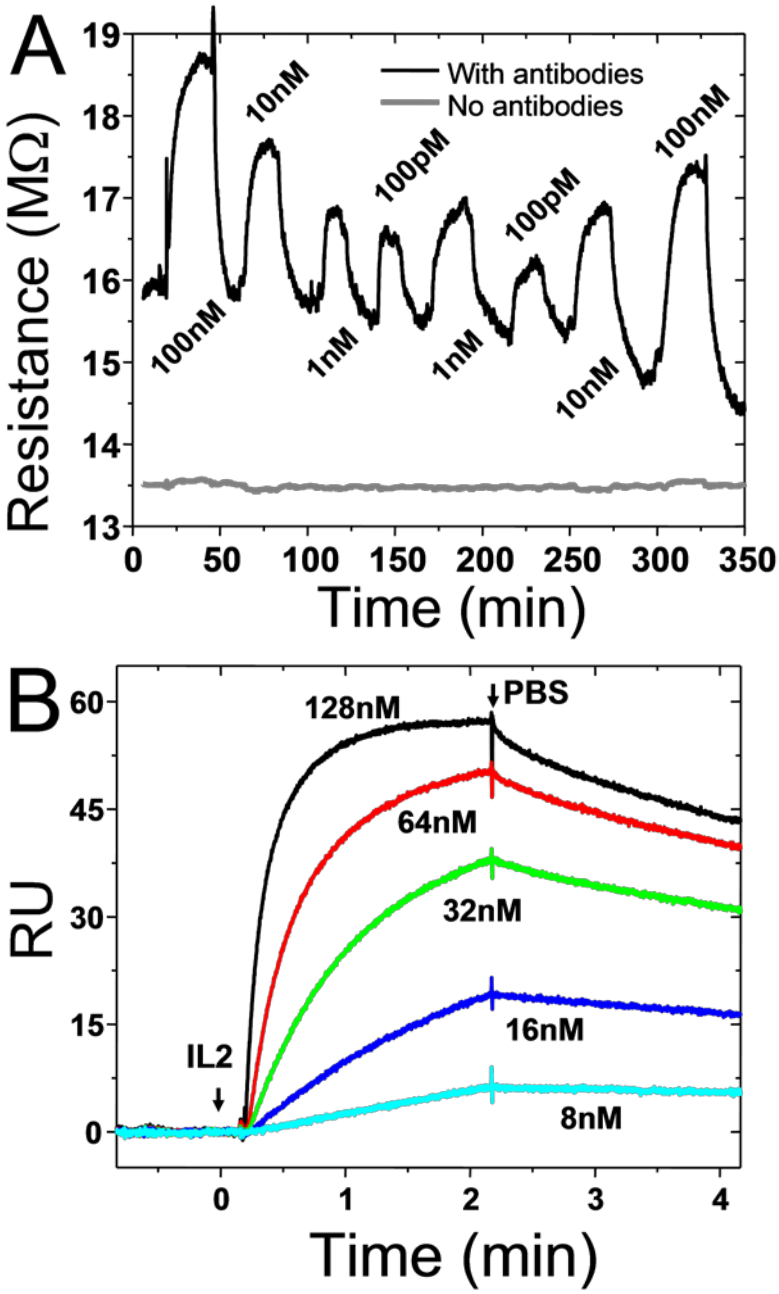

Figure 2.14 IL-2 sensing with dual channel device. (A) Real-time, differential sensing of human IL-2 in 10 μM PBS. The solutions containing IL-2 at different concentrations (100 nM, 10 nM, 1 nM, and 100 pM) were flowed sequentially over an active region of SiNWs which were functionalized with anti-human IL-2 antibodies (black curve), with the addition of 10 μM PBS after each IL-2 concentration to wash away bound proteins. Simultaneously, the same solutions were also introduced into a separate channel (Figure 2.13) containing SiNWs without antibodies on the surface (grey curve). (B) SPR of IL-2-anti IL-2 antibody interaction at different concentrations of IL-2. The flow rate was 30 μl/min.

nanowires to the binding of IL-2 is consistent with the majority surface charge of the protein. The isoelectric point of recombinant human IL-2 is between pH 6.5 and 7.5. Therefore in dilute PBS, pH ~ 6.0, there should be a prevalence of positive surface charges on the protein, leading to an increase in resistance of p-type silicon nanowires (Figs. 2.12 and 2.14).

The above protein-sensing experiments demonstrate that it is possible to engineer silicon nanowires to detect protein concentrations below the detection limit of other label-free methods, such as SPR (Fig. 2.14B). The detection of IL-2, which is a crucial cytokine of the immune system, is demonstrated. For more practical application of this technique, such as detecting low levels of cancer markers in the serum, it is necessary to address the Debye length issue. In the next section, we will discuss a method of utilizing peptides to detect proteins in higher ionic strength solution.

2.3.3 Protein sensing with peptide

As a first step, we showed the efficient immobilization of the FLAG peptide on the bulk silicon (100) surface by using X-ray photoelectron spectroscopy (XPS) (Fig. 2.3). A cleaned silicon (100) surface was treated with 2% (v/v) APMES to generate the amine-terminated surface (Surface 1 in Fig. 2.3A). Surface 1 was converted into an azide-terminated one through the coupling between an azide-containing unnatural amino acid and the amine on the surface (Surface 2 in Fig. 2.3A). Finally, the FLAG peptide was immobilized by alkyne-azide “click” cycloaddition (Surface 3 in Fig. 2.3A). The contact angles for amine, azide, and FLAG peptide surfaces were 72°, 73°, and 35° respectively. The significant decrease in contact angle after the click reaction suggests efficient peptide coupling to the surface. The presence of the azide group on Surface 2 can be identified

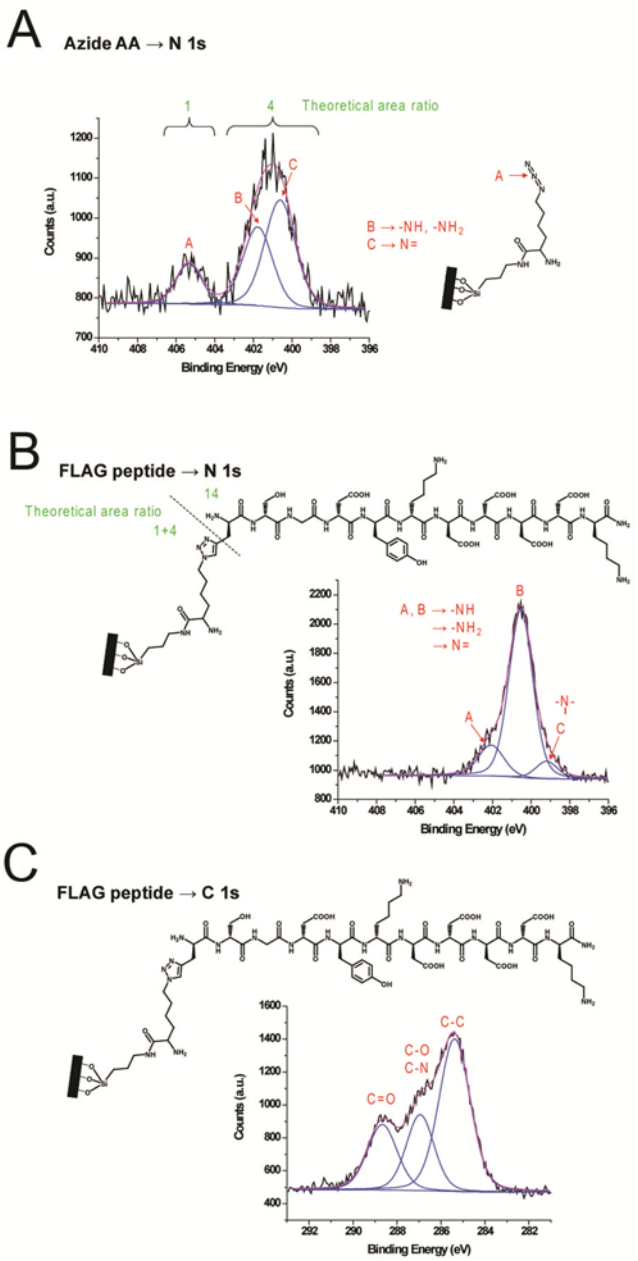

Figure 2.15 High-resolution XPS spectra of Surfaces 2 (A) and 3 (B and C), illustrating the coupling of the azide-containing unnatural amino acid and subsequently the FLAG peptide. A) N 1s region revealing the presence of azide on the surface by a growth of a small peak at 405 eV due to the central electron-withdrawing nitrogen atom. (B) N 1s region following the click reaction suggesting incorporation of the FLAG peptide on the azide-modified surface. The disappearance of the azide peak at 405 eV suggests that the click reaction has gone to completion. (C) C ls region displaying prominent C-N, C-O, and C=O peaks, compatible with peptide attachment to the surface

from the peak at 405 eV in the N 1s spectra of XPS, which is attributed to the central, electron-deficient nitrogen in the azide group (Fig. 2.3B). The disappearance of the same peak on Surface 3 explains ~ 100% conversion to the peptide-modified surface (Fig. 2.3B). By analyzing the ratio of the 400 eV and 405 eV peak areas in N 1s spectra, azide amino acid coverage in Surface 2 can be estimated as 73%, assuming 100% of APMES coverage, and the conversion to the peptide can be estimated as 100% [67] (Fig. 2.15). The growth of the 289 eV peak in C 1s spectra, which corresponds to C=O, a signature of peptides by XPS, also proves that the click reaction has proceeded (Fig. 2.15C).

To demonstrate the functionality of the peptide immobilized by click chemistry on silicon, a fluorescence-based bioassay in microfluidic channels was performed (Fig. 2.15). The amine-terminated surface was treated with azide-containing amino acid. Then a PDMS chip was bonded, and click reaction with the FLAG peptide was allowed to proceed in the microfluidic channel. As a control, channels 1 and 4 were filled with peptide solution without Cu^{I} catalyst and channels 2 and 5 were left as the azide-terminated surface. Channels 3 and 6 were treated with the FLAG peptide in the presence of the Cu^{I} catalysts. After the surface treatment in the microfluidic channels, anti-FLAG M2 antibodies and anti-human INFγ antibodies were filled into channels 1 to 3 and channels 4 to 6, respectively. After 1 h of incubation, secondary anti-mouse antibodies tagged with biotin were introduced into all channels and incubated for 1 hour. Then streptavidin coujugated with a Cy-5 fluorescence tag was reacted with the bound secondary anti-mouse antibodies. For all solutions containing antibodies, 1% BSA was included to prevent non-specific binding. Only channel 3, which was treated with FLAG peptide under the proper click condition and reacted with anti-FLAG M2 antibodies, showed fluorescence (Fig. 2.15A).

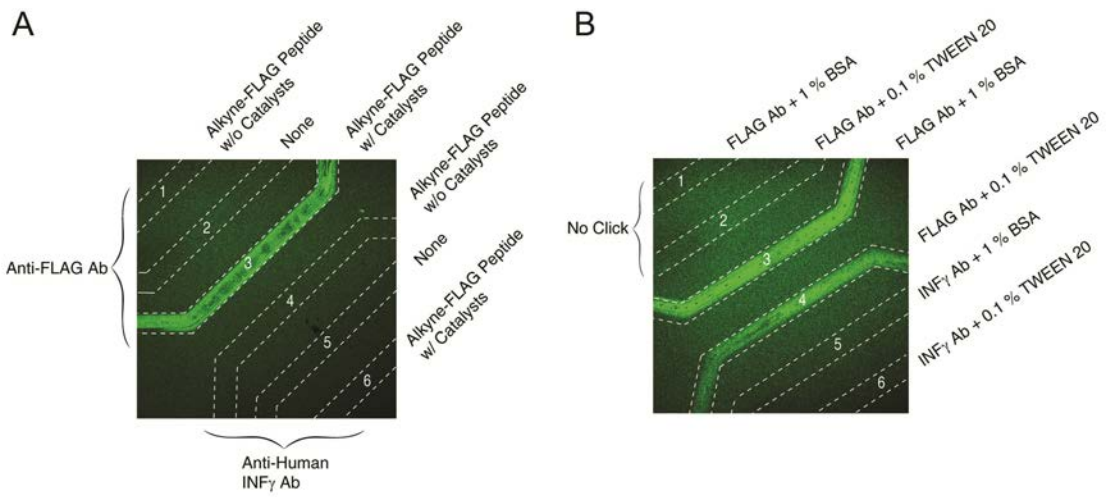

Figure 2.16 Fluorescence-based bioassay with FLAG peptides in microfluidic channels. (A) Assay result illustrating the immobilization of the FLAG peptides on a silicon surface by click chemistry. The amine-terminated silicon surface was converted into the azide-terminated surface before the PDMS chip was bonded. Only channels 3 and 6 were treated with the proper conditions for click chemistry. Anti-FLAG antibodies and anti-human INFγ antibodies were flowed through channels 1 to 3 and channels 4 to 6, respectively. 1% BSA was used as a blocking agent. (B) Assay result comparing the effect of 1% BSA and 0.1% Tween 20 as blocking agents. The surface was prepared as (A) but channels 3 to 6 were treated with the proper click chemistry condition.

From this result, it can be noticed that the presented surface treatment scheme works for efficient immobilization of synthetic capture agents on a silicon surface. Although the size of the FLAG peptide is small enough for the SiNW-FETs sensing in high ionic strength solution, non-specific binding of the large BSA molecules can significantly lower the accessibility of binding antibodies to the peptide on the surface of NWs due to steric effects. To prevent that problem, 0.1% Tween 20 was tested as an alternative blocking agent. The surface was treated as described above but only channels 1 and 2 were left as azide-terminated surface whereas all the other channels were treated with FLAG peptide. The result shows that Tween 20 can also minimize the non-specific binding as effectively as BSA (Fig. 2.15B).

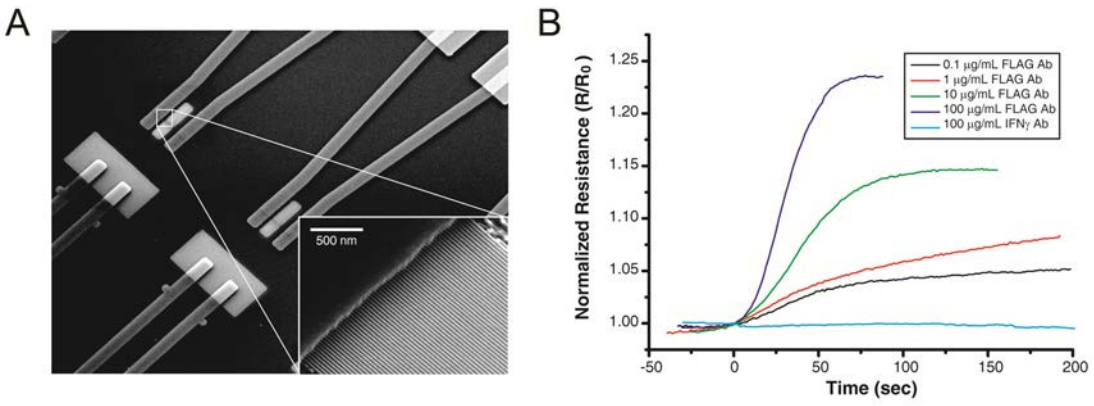

Figure 2.17 Scanning electron micrograph (SEM) image of the NW-FET device and sensing result. A) An SEM image of the SiNWs-based FET biosensor. One set of sensors is placed in a microfluidic channel. (Inset) Zoomed-in image of the NWs. Each sensing component is composed of about 65 NWs. B) NWs sensing results with anti-FLAG antibodies at different concentrations. 100 μg/mL of anti-human INFγ antibodies were also tested as a reference and showed negligible change of the resistance. All samples started to react with the actual sensing component at t = 0. For all experiments, 0.1 % Tween 20 was used as a blocking agent.

By utilizing peptides as a capture agent and click chemistry as a surface treatment method, we can sense anti-FLAG antibodies with SiNW-FETs in 0.1×PBS, which is 15 mM solution (Fig. 2.17). The Debye screening length of this high ionic strength solution is about 2.3 nm.[68] The SiNWs were fabricated by the superlattice nanowire pattern transfer (SNAP) method.[35] Then the SiNWs were sectioned into about 65 NWs and metal electrodes were patterned by photolithography technique (Fig. 2.17A). Up to 0.1 μg/mL (~ 666 pM) of anti-FLAG M2 antibody was clearly sensed whereas 100 μg/mL (~ 666 nM) of anti-human INFγ□antibody did not give any noticable signal (Fig. 2.17B). Although the sensitivity of the device was not that high, it can be enhanced by optimizing fabrication

conditions such as the doping concentration. Detection of target proteins in fM sensitivity is reported from other groups [21, 30] and further work is in progress to achieve high sensitivity.

Because high-salt buffer solution provides a better condition for the activity of biomolecules, and considering the efforts on developing synthetic capture agents such as peptides, peptoid and small molecules,[25, 69–71] these data suggest that the peptide immobilization via click chemistry may offer more practical applications of the SiNW-FETs in basic studies of biological reaction as well as detection.

2.4 Conclusions

Real-time label-free detection of DNA and proteins with SiNWs was performed. Primary DNA was electrostatically adsorbed onto an amine-terminated SiNW surface and hybridized to the complementary strand in a microfluidics channel under flow. Electrostatic adsorption of single-stranded DNA to poly-L-lysine-coated surface has previously been electronically detected at nanomolar concentrations with capacitive methods on lowly doped Si electrodes in 0.015 M solution.[72] The ability to detect DNA under physiological conditions, as demonstrated in this work, is of significance, as it may allow the direct use of biological samples such as serum or tissue culture media. It is likely that because the primary DNA is electrostatically bound and hybridization occurs very close to NW surface, Debye screening does not prevent SiNW-based detection.

SiNWs with significantly reduced oxide coverage exhibited enhanced solution FET characteristics (Fig. 2.6) when compared to SiNWs characterized by a native SiO_2 surface passivation. Oxide-covered, highly doped SiNWs were designed to exhibit a similar

dynamic range of DNA detection as the best near-infrared imaging SPR technique[73](–10 nM for 18 mer, corresponding to ~ 10^{11} molecules/cm^2). When identical nanowires were functionalized by the UV-initiated radical chemistry method, resulting in near-elimination of the Si-SiO_2 interface, the limit of detection was increased by two orders of magnitude, with an accompanying increase in the dynamic range. This result highlights the importance of controlling surface chemistry of SiNWs for their optimization as biological sensors. In the future, surface chemistries yielding higher coverage than UV-initiated alkylation may be utilized to passivate and electrochemically convert SiNWs into arrays for multiparameter analysis.[42, 74]

Sensing of an important cytokine, interleukin-2, has also been performed. Protein detection is significantly limited by the size of the capture agent. Using antibodies poses a limitation on the ionic strength of the buffer containing the analyte. To circumvent this limitation, we propose using peptide as alternative high-affinity protein probes. The application demonstrated in this chapter, detecting FLAG antibody with FLAG peptide, is a well-known system and just shows the feasibility for now. Thus a general scheme to screen and make synthetic capture agents on demand must be developed.[25] However, a combination of an appropriate doping level and surface chemistry will undoubtedly allow the detection down to a sub-picomolar regime, which is more than sufficient for most relevant clinical applications.

A model that is consistent with both the standard Langmuir binding model and with the fundamentals of semiconductor physics is developed. Kinetic parameters and analyte concentrations that are consistent with SPR values may be extracted from the silicon nanowire experiments. The potential for SiNW sensors to quantitate the concentrations of

low-abundance biomolecules within physiologically relevant environments is an intriguing one, and it is worth vigorously pursuing this possibility. The most useful application of our model would be in extracting otherwise unknown concentration values once k_{on} and k_{off} values are known. As demonstrated here, SiNW sensors can be used for label-free biomolecule detection at concentrations significantly below the limits of detection for SPR. The robustness of the fabrication technique (SNAP) employed here, which yields nanowire sensors that exhibit reproducible and highly tunable behavior, holds a promise for the future integration of this technology within the clinical setting.

2.5 References

1. Kong, J.; Franklin, N. R.; Zhou, C. W.; Chapline, M. G.; Peng, S.; Cho, K. J.; Dai, H. J., Nanotube molecular wires as chemical sensors. *Science* **2000,** 287, (5453), 622–625.
2. Patolsky, F.; Timko, B. P.; Zheng, G. F.; Lieber, C. M., Nanowire-based nanoelectronic devices in the life sciences. *MRS Bulletin* **2007,** 32, (2), 142–149.
3. Park, S. J.; Taton, T. A.; Mirkin, C. A., Array-based electrical detection of DNA with nanoparticle probes. *Science* **2002,** 295, (5559), 1503–1506.
4. Ziegler, C., Nanotechnologies for the biosciences. *Analytical and Bioanalytical Chemistry* **2004,** 379, (7–8), 903–903.
5. Lasseter, T. L.; Cai, W.; Hamers, R. J., Frequency-dependent electrical detection of protein binding events. *Analyst* **2004,** 129, (1), 3–8.
6. Davidson, E. H.; Rast, J. P.; Oliveri, P.; Ransick, A.; Calestani, C.; Yuh, C. H.; Minokawa, T.; Amore, G.; Hinman, V.; Arenas-Mena, C.; Otim, O.; Brown, C. T.; Livi, C. B.; Lee, P. Y.; Revilla, R.; Rust, A. G.; Pan, Z. J.; Schilstra, M. J.; Clarke, P. J. C.;

Arnone, M. I.; Rowen, L.; Cameron, R. A.; McClay, D. R.; Hood, L.; Bolouri, H., A genomic regulatory network for development. *Science* **2002,** 295, (5560), 1669–1678.

7. Kitano, H., Systems biology: A brief overview. *Science* **2002,** 295, (5560), 1662–1664.
8. Hood, L.; Heath, J. R.; Phelps, M. E.; Lin, B. Y., Systems biology and new technologies enable predictive and preventative medicine. *Science* **2004,** 306, (5696), 640–643.
9. Chen, R. J.; Bangsaruntip, S.; Drouvalakis, K. A.; Kam, N. W. S.; Shim, M.; Li, Y. M.; Kim, W.; Utz, P. J.; Dai, H. J., Noncovalent functionalization of carbon nanotubes for highly specific electronic biosensors. *Proceedings of the National Academy of Sciences of the United States of America* **2003,** 100, (9), 4984–4989.
10. Star, A.; Tu, E.; Niemann, J.; Gabriel, J. C. P.; Joiner, C. S.; Valcke, C., Label–free detection of DNA hybridization using carbon nanotube network field-effect transistors. *Proceedings of the National Academy of Sciences of the United States of America* **2006,** 103, (4), 921–926.
11. Besteman, K.; Lee, J. O.; Wiertz, F. G. M.; Heering, H. A.; Dekker, C., Enzyme-coated carbon nanotubes as single-molecule biosensors. *Nano Letters* **2003,** 3, (6), 727–730.
12. Maehashi, K.; Katsura, T.; Kerman, K.; Takamura, Y.; Matsumoto, K.; Tamiya, E., Label-free protein biosensor based on aptamer-modified carbon nanotube field-effect transistors. *Analytical Chemistry* **2007,** 79, (2), 782–787.
13. Cui, Y.; Wei, Q. Q.; Park, H. K.; Lieber, C. M., Nanowire nanosensors for highly sensitive and selective detection of biological and chemical species. *Science* **2001,** 293, (5533), 1289–1292.
14. Hahm, J.; Lieber, C. M., Direct ultrasensitive electrical detection of DNA and DNA sequence variations using nanowire nanosensors. *Nano Letters* **2004,** 4, (1), 51–54.

15. Li, Z.; Chen, Y.; Li, X.; Kamins, T. I.; Nauka, K.; Williams, R. S., Sequence-specific label-free DNA sensors based on silicon nanowires. *Nano Letters* **2004,** 4, (2), 245–247.

16. Li, C.; Curreli, M.; Lin, H.; Lei, B.; Ishikawa, F. N.; Datar, R.; Cote, R. J.; Thompson, M. E.; Zhou, C. W., Complementary detection of prostate-specific antigen using ln(2)O(3) nanowires and carbon nanotubes. *Journal of the American Chemical Society* **2005,** 127, (36), 12484–12485.

17. Ramanathan, K.; Bangar, M. A.; Yun, M.; Chen, W.; Myung, N. V.; Mulchandani, A., Bioaffinity sensing using biologically functionalized conducting-polymer nanowire. *Journal of the American Chemical Society* **2005,** 127, (2), 496–497.

18. Lud, S. Q.; Nikolaides, M. G.; Haase, I.; Fischer, M.; Bausch, A. R., Field effect of screened charges: Electrical detection of peptides and proteins by a thin-film resistor. *Chemphyschem* **2006,** 7, (2), 379–384.

19. Neff, P. A.; Wunderlich, B. K.; Lud, S. Q.; Bausch, A. R., Silicon-on-insulator based thin film resistors for quantitative biosensing applications. *Physica Status Solidi A—Applications and Materials Science* **2006,** 203, (14), 3417–3423.

20. Israelachvilli, J., *Intermolecular and Surface Forces*. Academic Press: London, 1985.

21. Zheng, G. F.; Patolsky, F.; Cui, Y.; Wang, W. U.; Lieber, C. M., Multiplexed electrical detection of cancer markers with nanowire sensor arrays. *Nature Biotechnology* **2005,** 23, (10), 1294–1301.

22. Okahata, Y.; Kawase, M.; Niikura, K.; Ohtake, F.; Furusawa, H.; Ebara, Y., Kinetic measurements of DNA hybridisation an an oligonucleotide-immobilized 27-MHz quartz crystal microbalance. *Analytical Chemistry* **1998,** 70, (7), 1288–1296.

23. Naffin, J. L.; Han, Y.; Olivos, H. J.; Reddy, M. M.; Sun, T.; Kodadek, T., Immobilized peptides as high-affinity capture agents for self-associating proteins. *Chemical Biology* **2003,** 10, (3), 251–259.

24. Wegner, G. J.; Lee, H. J.; Corn, R. M., Characterization and optimization of peptide arrays for the study of epitope-antibody interactions using surface plasmon resonance imaging. *Analytical Chemistry* **2002,** 74, (20), 5161–5168.

25. Agnew, H. D.; Rohde, R. D.; Millward, S. W.; Nag, A.; Yeo, W. S.; Hein, J. E.; Pitram, S. M.; Tariq, A. A.; Burns, V. M.; Krom, R. J.; Fokin, V. V.; Sharpless, K. B.; Heath, J. R., Iterative in situ click chemistry creates antibody-like protein-capture agents. *Angewandte Chemie International Edition* **2009,** 48, (27), 4944–4948.

26. Kolb, H. C.; Finn, M. G.; Sharpless, K. B., Click Chemistry: Diverse Chemical Function from a Few Good Reactions. *Angewandte Chemie International Edition* **2001,** 40, (11), 2004–2021.

27. Li, Z.; Rajendran, B.; Kamins, T. I.; Li, X.; Chen, Y.; Williams, R. S., Silicon nanowires for sequence–specific DNA sensing: device fabrication and simulation. *Applied Physics A—Materials Science & Processing* **2005,** 80, (6), 1257–1263.

28. Vieu, C.; Carcenac, F.; Pepin, A.; Chen, Y.; Mejias, M.; Lebib, A.; Manin-Ferlazzo, L.; Couraud, L.; Launois, H., Electron beam lithography: resolution limits and applications. *Applied Surface Science* **2000,** 164, 111–117.

29. Yang, P. D., The chemistry and physics of semiconductor nanowires. *MRS Bulletin* **2005,** 30, (2), 85–91.

30. Stern, E.; Klemic, J. F.; Routenberg, D. A.; Wyrembak, P. N.; Turner-Evans, D. B.; Hamilton, A. D.; LaVan, D. A.; Fahmy, T. M.; Reed, M. A., Label-free

immunodetection with CMOS-compatible semiconducting nanowires. *Nature* **2007,** 445, (7127), 519–522.

31. Gao, Z.; Agarwal, A.; Trigg, A. D.; Singh, N.; Fang, C.; Tung, C. H.; Fan, Y.; Buddharaju, K. D.; Kong, J., Silicon Nanowire Arrays for Label-Free Detection of DNA. *Analytical Chemistry* **2007**, 79 (9), 3291–3297.
32. Heath, J. R.; Legoues, F. K., A Liquid Solution Synthesis of Single-Crystal Germanium Quantum Wires. *Chemical Physics Letters* **1993,** 208, (3–4), 263–268.
33. Morales, A. M.; Lieber, C. M., A laser ablation method for the synthesis of crystalline semiconductor nanowires. *Science* **1998,** 279, (5348), 208–211.
34. Chung, S. W.; Yu, J. Y.; Heath, J. R., Silicon nanowire devices. *Applied Physics Letters* **2000,** 76, (15), 2068–2070.
35. Melosh, N. A.; Boukai, A.; Diana, F.; Gerardot, B.; Badolato, A.; Petroff, P. M.; Heath, J. R., Ultrahigh-density nanowire lattices and circuits. *Science* **2003,** 300, (5616), 112–115.
36. Beckman, R. A.; Johnston-Halperin, E.; Melosh, N. A.; Luo, Y.; Green, J. E.; Heath, J. R., Fabrication of conducting Si nanowire arrays. *Journal of Applied Physics* **2004,** 96, (10), 5921–5923.
37. Wikswo, J. P.; Prokop, A.; Baudenbacher, F.; Cliffel, D.; Csukas, B.; Velkovsky, M., Engineering challenges of BioNEMS: the integration of microfluidics, micro- and nanodevices, models and external control for systems biology. *IEEE Proceedings—Nanobiotechnology* **2006,** 153, (4), 81–101.

38. Yablonovitch, E.; Allara, D. L.; Chang, C. C.; Gmitter, T.; Bright, T. B., Unusually Low Surface-Recombination Velocity on Silicon and Germanium Surfaces. *Physical Review Letters* **1986,** 57, (2), 249–252.

39. Sham, T. K.; Naftel, S. J.; Kim, P. S. G.; Sammynaiken, R.; Tang, Y. H.; Coulthard, I.; Moewes, A.; Freeland, J. W.; Hu, Y. F.; Lee, S. T., Electronic structure and optical properties of silicon nanowires: A study using X-ray excited optical luminescence and X-ray emission spectroscopy. *Physical Review B* **2004,** 70, 045313.

40. Webb, L. J.; Lewis, N. S., Comparison of the electrical properties and chemical stability of crystalline silicon(111) surfaces alkylated using grignard reagents or olefins with Lewis acid catalysts. *Journal of Physical Chemistry B* **2003,** 107, (23), 5404–5412.

41. Bansal, A.; Lewis, N. S., Stabilization of Si photoanodes in aqueous electrolytes through surface alkylation. *Journal of Physical Chemistry B* **1998,** 102, (21), 4058–4060.

42. Bunimovich, Y. L.; Ge, G. L.; Beverly, K. C.; Ries, R. S.; Hood, L.; Heath, J. R., Electrochemically programmed, spatially selective biofunctionalization of silicon wires. *Langmuir* **2004,** 20, (24), 10630–10638.

43. Haick, H.; Hurley, P. T.; Hochbaum, A. I.; Yang, P. D.; Lewis, N. S., Electrical characteristics and chemical stability of non-oxidized, methyl-terminated silicon nanowires. *Journal of the American Chemical Society* **2006,** 128, (28), 8990–8991.

44. Terry, J.; Mo, R.; Wigren, C.; Cao, R. Y.; Mount, G.; Pianetta, P.; Linford, M. R.; Chidsey, C. E. D., Reactivity of the H-Si (111) surface. *Nuclear Instruments & Methods in Physics Research Section B—Beam Interactions with Materials and Atoms* **1997,** 133, (1–4), 94–101.

45. Effenberger, F.; Gotz, G.; Bidlingmaier, B.; Wezstein, M., Photoactivated preparation and patterning of self-assembled monolayers with 1-alkenes and aldehydes on silicon hydride surfaces. *Angewandte Chemie International Edition* **1998,** 37, (18), 2462–2464.

46. Boukherroub, R.; Wayner, D. D. M., Controlled functionalization and multistep chemical manipulation of covalently modified Si(111) surfaces. *Journal of the American Chemical Society* **1999,** 121, (49), 11513–11515.

47. Cicero, R. L.; Linford, M. R.; Chidsey, C. E. D., Photoreactivity of unsaturated compounds with hydrogen-terminated silicon(111). *Langmuir* **2000,** 16, (13), 5688–5695.

48. Streifer, J. A.; Kim, H.; Nichols, B. M.; Hamers, R. J., Covalent functionalization and biomolecular recognition properties of DNA-modified silicon nanowires. *Nanotechnology* **2005,** 16, (9), 1868–1873.

49. Jonsson, U.; Fagerstam, L.; Ivarsson, B.; Johnsson, B.; Karlsson, R.; Lundh, K.; Lofas, S.; Persson, B.; Roos, H.; Ronnberg, I.; Sjolander, S.; Stenberg, E.; Stahlberg, R.; Urbaniczky, C.; Ostlin, H.; Malmqvist, M., Real-Time Biospecific Interaction Analysis Using Surface-Plasmon Resonance and a Sensor Chip Technology. *Biotechniques* **1991,** 11, (5), 620–&.

50. Wang, D. W.; Sheriff, B. A.; Heath, J. R., Silicon p-FETs from ultrahigh density nanowire arrays. *Nano Letters* **2006,** 6, (6), 1096–1100.

51. Duffy, D. C.; McDonald, J. C.; Schueller, O. J. A.; Whitesides, G. M., Rapid prototyping of microfluidic systems in poly(dimethylsiloxane). *Analytical Chemistry* **1998,** 70, (23), 4974–4984.

52. Unger, M. A.; Chou, H. P.; Thorsen, T.; Scherer, A.; Quake, S. R., Monolithic microfabricated valves and pumps by multilayer soft lithography. *Science* **2000,** 288, (5463), 113–116.

53. Haber, J. A.; Lewis, N. S., Infrared and X-ray photoelectron spectroscopic studies of the reactions of hydrogen-terminated crystalline Si(111) and Si(100) surfaces with Br-2, I-2, and ferrocenium in alcohol solvents. *Journal of Physical Chemistry B* **2002,** 106, (14), 3639–3656.

54. Himpsel, F. J.; McFeely, F. R.; Talebibrahimi, A.; Yarmoff, J. A.; Hollinger, G., Microscopic Structure of the SiO_2/Si Interface. *Physical Review B* **1988,** 38, (9), 6084–6096.

55. Chenault, H. K., Dahmer, J. and Whitesides, G.M., Kinetic resolution of unnatural and rarely occurring amino acids: enantioselective hydrolysis of N-acyl amino acids catalyzed by acylase I. *Journal of the American Chemical Society* **1989,** 111.

56. van Hest, J. C. M., Kiick, K.L. and Tirrell, D.A., Efficient incorporation of unsaturated methionine analogues intoproteins in vivo. *Journal of the American Chemical Society* **2000,** 122.

57. Lee, H.-S., Park, J.-S., Kim, B.M. and Gellman, S.H. , Efficient synthesis of enantiomerically pure ♌2-amino acids via chiral isoxazolidinones. *Journal of Organic Chemistry* **2003,** 68.

58. Hu, K.; Fan, F. R. F.; Bard, A. J.; Hillier, A. C., Direct measurement of diffuse double-layer forces at the semiconductor/electrolyte interface using an atomic force microscope. *Journal of Physical Chemistry B* **1997,** 101, (41), 8298–8303.

59. Cui, Y.; Duan, X. F.; Hu, J. T.; Lieber, C. M., Doping and electrical transport in silicon nanowires. *Journal of Physical Chemistry B* **2000,** 104, (22), 5213–5216.

60. Cheng, M. M.-C.; Cuda, G.; Bunimovich, Y. L.; Gaspari, M.; Heath, J. R.; Hill, H. D.; Mirkin, C. A.; Nijdam, A. J.; Terracciano, R.; Thundat, T.; Ferrari, M., Nanotechnologies for biomolecular detection and medical diagnostics. *Current Opinion in Chemical Biology* **2006,** 10, (1), 11–19.

61. Beckman, R.; Johnston-Halperin, E.; Luo, Y.; Green, J. E.; Heath, J. R., Bridging dimensions: Demultiplexing ultrahigh-density nanowire circuits. *Science* **2005,** 310, (5747), 465–468.

62. Stenberg, E.; Persson, B.; Roos, H.; Urbaniczky, C., Quantitative-Determination of Surface Concentration of Protein with Surface-Plasmon Resonance Using Radiolabeled Proteins. *Journal of Colloid and Interface Science* **1991,** 143, (2), 513–526.

63. Yu, F.; Yao, D. F.; Knoll, W., Oligonucleotide hybridization studied by a surface plasmon diffraction sensor (SPDS). *Nucleic Acids Research* **2004,** 32, (9).

64. Peterson, A. W.; Heaton, R. J.; Georgiadis, R. M., The effect of surface probe density on DNA hybridization. *Nucleic Acids Research* **2001,** 29, (24), 5163–5168.

65. Lemeshko, S. V.; Powdrill, T.; Belosludtsev, Y. Y.; Hogan, M., Oligonucleotides form a duplex with non-helical properties on a positively charged surface. *Nucleic Acids Research* **2001,** 29, (14), 3051–3058.

66. Zimmermann, M.; Delamarche, E.; Wolf, M.; Hunziker, P., Modeling and optimization of high-sensitivity, low-volume microfluidic-based surface immunoassays. *Biomedical Microdevices* **2005,** 7, (2), 99–110.

67. Collman, J. P.; Devaraj, N. K.; Eberspacher, T. P.; Chidsey, C. E., Mixed azide-terminated monolayers: a platform for modifying electrode surfaces. *Langmuir* **2006,** 22, (6), 2457–2464.

68. Stern, E.; Wagner, R.; Sigworth, F. J.; Breaker, R.; Fahmy, T. M.; Reed, M. A., Importance of the debye screening length on nanowire field effect transistor sensors. *Nano Letters* **2007,** 7, (11), 3405–9.

69. Alluri, P. G.; Reddy, M. M.; Bachhawat-Sikder, K.; Olivos, H. J.; Kodadek, T., Isolation of Protein Ligands from Large Peptoid Libraries. *Journal of the American Chemical Society* **2003,** 125, (46), 13995–14004.

70. Bachhawat-Sikder, K.; Kodadek, T., Mixed-Element Capture Agents: A Simple Strategy for the Construction of Synthetic, High-Affinity Protein Capture Ligands. *Journal of the American Chemical Society* **2003,** 125, (32), 9550–9551.

71. Enander, K., Dolphin, G.T., Liedberg, B., Lundström, I., Baltzer, L., A Versatile Polypeptide Platform for Integrated Recognition and Reporting: Affinity Arrays for Protein-Ligand Interaction Analysis. *Chemistry—A European Journal* **2004,** 10, (10), 2375–2385.

72. Fritz, J.; Cooper, E. B.; Gaudet, S.; Sorger, P. K.; Manalis, S. R., Electronic detection of DNA by its intrinsic molecular charge. *Proceedings of the National Academy of Sciences of the United States of America* **2002,** 99, (22), 14142–14146.

73. Nelson, B. P.; Grimsrud, T. E.; Liles, M. R.; Goodman, R. M.; Corn, R. M., Surface plasmon resonance imaging measurements of DNA and RNA hybridization adsorption onto DNA microarrays. *Analytical Chemistry* **2001,** 73, (1), 1–7.

74. Rohde, R. D.; Agnew, H. D.; Yeo, W. S.; Bailey, R. C.; Heath, J. R., A non-oxidative approach toward chemically and electrochemically functionalizing Si(111). *Journal of the American Chemical Society* **2006,** 128, (29), 9518–9525.